Treball de Fi de Grau

Grau en Enginyeria de Materials

3D Printing with advanced ceramic materials

MEMÒRIA

Autor: Lara de Luis Chueca

Director/s: Joan Josep Roa Rovira

Ponent: Emilio Jiménez Piqué

Convocatòria: Juny 2016

Escola Tècnica Superior

d'Enginyeria Industrial de Barcelona

Abstract

Due to the aging of the population and the need for maintaining masticatory functionality during their life span, the number of dental replacements is growing, substituting natural teeth by artificial crows, bridges and implants. In fact, in recent years the number of teeth replacement has increased, and one of the relatively new and preferred dental materials is the tetragonal zirconia doped with 3% mol yttria (3Y-ZrO_2, also referred to us like 3Y-TZP). This material is in vogue due to its aesthetic appearance, bio-inertness and mechanical properties for dental crowns and bridges (with a porcelain veneer). However, until recently scaffold design was limited to conventional manufacturing methods (i.e., starting from a bulk ceramic body and subtracting the material step by step in order to generate the scaffold's final outer shape). Nowadays, new technologies enable adding up complex three-dimensional structures layer by layer. Powder based rapid prototyping technique in such a versatile method with unique flexibility in material and geometry.

In this work, microstructural mixtures of 3Y-TZP and CeO_2 based ceramic materials were design and produced by Rapid Prototyping (3D printing geometries) with the main goal to evaluate a possible correlation between their microstructural and mechanical properties. The results were compared and discussed in terms of density, porosity, grain size, absorbance, transmittance, reflectance, hardness and cyclic indentation as a function of the sintering temperature. A detailed characterization of the microstructure was performed by Confocal Laser Microscopy and Field Emission Scanning Electron Microscopy.

Index

1. Introduction

Along this introductory chapter, the basic and necessary concepts to understand this Bachelor's project will be presented in detail. In this chapter is possible to find the main properties of advanced ceramic materials; mainly composite ceramic materials composed zirconia and ceria. After that, his rapid prototyping technique (3D-printing technique) will be presented as new techniques to develop complex geometries among other relevant concepts for understand perfectly the other chapters of this Bachelor's project.

1.1. Advanced Materials

Materials that are employed in high-technology applications are sometimes well-known as *advanced materials*. These families of materials are typically traditional materials whose properties have been improved, and, also newly developed. Furthermore, they may be constituted from different material types, and are normally expensive. Advanced materials include semiconductors, biomaterials and what we may term "materials for the future" (that is, smart materials and nanoengineered materials) [1]. For this final **Bachelor's project** we will focus on **biomaterials group**.

Biomaterials are used in components implanted into the human body as a replacement of diseased or damaged body parts. These materials must not produce toxic substances and must be compatible with body tissues. As biomaterials is possible to find materials from all the families like metals, ceramics, polymers, composites and semiconductors [1]. This Bachelor's project is focused in advanced bio-ceramic materials, more concretely zirconium oxide also known as zirconia (ZrO_2) and cerium oxide, or what is the same, ceria (CeO_2). In the following sections, we extensively explain each ceramic material (Zirconia and Ceria in **sections 1.1.1** and **1.1.2**), taking especial attention in their microstructure, crystallographic structure as well as their mechanical properties.

1.1.1. Zirconia

Zirconia (ZrO_2) is chemically an oxide and technologically a ceramic material. This is one of the most important technological materials due to its diverse combination of their high hardness and Young's modulus, its chemical inert and stable under aggressive atmospheres, low friction coefficient wear resistance, ionic conductivity, mechanical resistance and moderate fracture

toughness.

However, this particular material presents a metastable tetragonal phase at room temperature. By mixing zirconia with other metallic oxides, which create vacancies inside the crystalline structure, is possible to obtain ceramic material more stable than the ZrO_2. In this regard, one of the most common stabilizing agents is the yttrium oxide, Y_2O_3 [2], which helps to stabilize the tetragonal phase at room temperature. This material also known as tetragonal zirconia polycrystal (TZP) is presently the most bio-ceramic material studied during the last decade.

1.1.1.1. Crystallographic phases

Phase transformation of zirconia is a martensite type. This process is characterized by a transformation at a certain range of temperature and produces changes in the shape of the nucleus as well as a volume expansion ranged between 4 to 5 %. The intensity of the martensitic phase transformation is mainly affected by several factors, like the grain size, shape, amount of stabilizing agents, among other factors extensively explained in Ref. [3].

Pure zirconia presents three different polymorphic structures depending on their working and/or processing temperature:

- **Cubic phase** has a fluorite structure type (face-centered cubic structure, f.c.c, see **Figure 1.1.1a**) and is stable from a wide range of temperatures (form 2370ºC to the melting point, 2680ºC). The density for this structure is around 6.09 g/cm^3 [4].

- **Tetragonal phase** is stable for temperatures from 1150ºC to 2370ºC, and has a primitive body centered cell, b.c.c (see **Figure 1.1.1b**). The density for this structure is around 6.10 g/cm^3 [4].

- For temperatures under 850ºC the most stable structure is the **monoclinic phase**, as is depicted in **Figure 1.1.1c**. The density for this phase is 5.83 g/cm^3 [4].

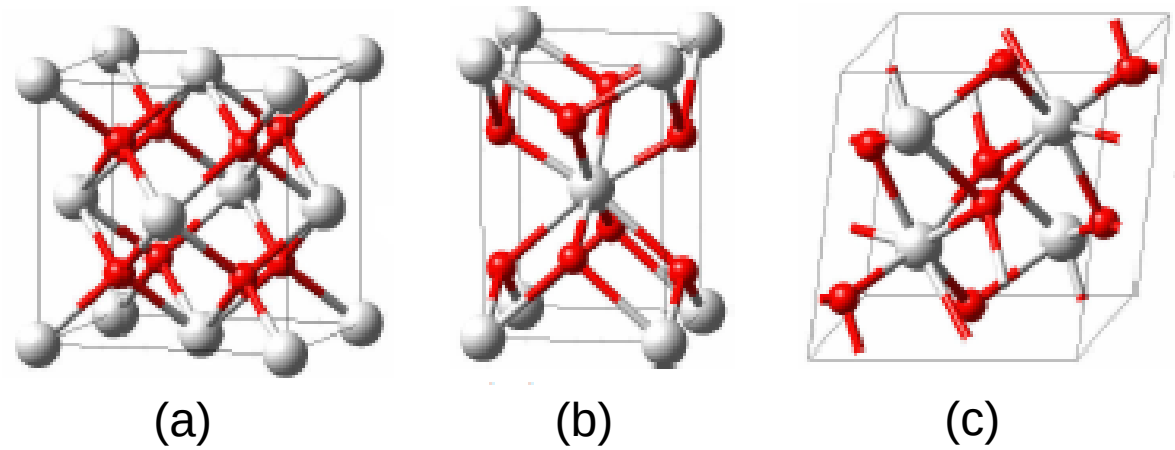

Figure 1.1.1 – *Main crystallographic structures for the ZrO_2. (a) Cubic, (b) tetragonal and (c) monoclinic phase [5].*

The most important transformation process is from tetragonal phase to monoclinic phase (*t*→*m*), which produces a martensitic transformation. This phase transformation is the main responsible of the cracking resistance improvement, as well as the degradation phenomenon that will be analyzed afterwards.

This martensitic transformation increases the toughness due to the activated tension on the tip's fissure [2], see **Figure 1.1.2**. This phenomenon opposes to the volumetric dilatation when the temperature goes down, and this causes the fissures closing due to the compressive stresses located in the tip's fissure. This effect produces a fracture toughness increases due to the reduction of the interior defects number [6].

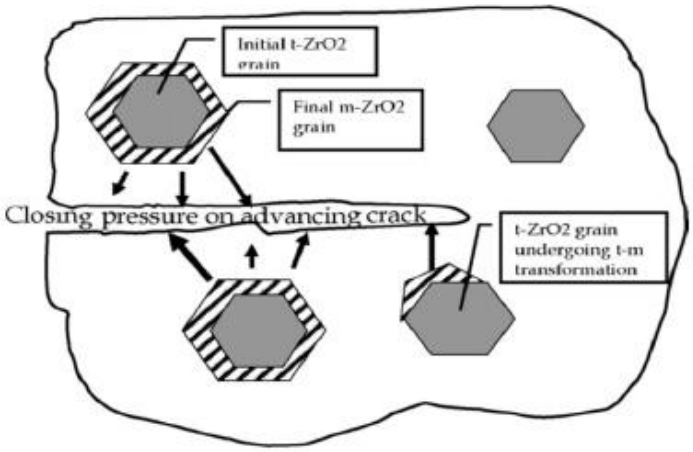

Figure 1.1.2 – *Schematic representing the main responsible effect which increases fracture toughness for ZrO_2 materials [6].*

1.1.1.2. Hydrothermal degradation

The ageing, hydrothermal degradation or low thermal degradation (LTD) occurs by a slow surface transformation to monoclinic phase in the presence of water or water vapor at low temperatures (≈ 132 - 134ºC). It causes the phase transformation from tetragonal to monoclinic. This process starts firstly in isolated grains on the surface by a stress corrosion type mechanism, and causes micro- cracking due to the increase in volume. After that, it propagates from the exterior to the interior of the material. This transformation mechanism is presented in **Figure 1.1.3** [7].

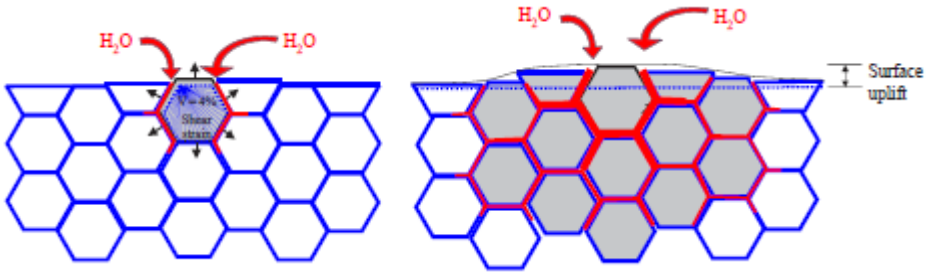

Figure 1.1.3 – *Scheme of the ageing process [7].*

1.1.1.3. Mechanical properties

Ceramic materials are inherently resilient to oxidation and deterioration at elevated temperatures. Furthermore, they present a high hardness value which makes the ceramic materials considerable brittle, mainly presenting a brittle fracture. In this sense, these types of materials present a low and a wide range of fracture toughness (K_{IC}) values typically ranged between 1 and 5 MPa√m. It is necessary to highlight, that during the last decade, the fracture toughness for ceramic materials have been improved significantly by adding reinforcing particles like fibers or whiskers of different ceramic nature. By doing this, the fracture toughness has been increased considerable by a factor of 4, reaching values ranging between 6 and 20 MPa√m [1]. This is owing to the interactions between advancing cracks and dispersed phase particles. The fracture mechanisms in terms of crack initiation, which normally starts in the matrix phase, but its propagation is impeded by this secondary phase (particles, fibers or whiskers).

In our particular case of interest, Zirconia presents similar mechanical properties to those of stainless steel. Its bend strength can be as high as 900-1200 MPa and its compressive strength is about 2000 MPa [2]. This material also works well under cyclical stresses as it was

previously reported in Ref. [8]. **Table 1.1.1** summarizes the main mechanical properties for the zirconia

Table 1.1.1 – *Zirconia mechanical properties [6].*

Mechanical Properties	Value
Density	6.05 g/cm^3
Hardness	1200 HV
Bend strength	900-1200 MPa
Compressive strength	2000 MPa
Fracture toughness	7-10 MPa$\sqrt{m}$
Young's modulus	210 GPa
Thermalexpansion coefficient	11x10^{-5} 1/K

1.1.1.4. Applications

Zirconia has multiple commercial applications among which it is important to stress its use as abrasive. Is possible to find zirconia as valves, oxygen sensors, cutting tools, combustible cells, sheet metal forming guides, thermal barrier coatings and finally as a dental implants and dental prosthesis, which is the most known application for zirconia, and the relevant one for this work Bachelor's project. In this sense, due to the high percentage of cases about problems with dental implants about toxic and allergic reactions to certain alloys, patients and dentists have been looking for metal-free tooth-colored restorations. At the same time, the development of new high strength dental ceramics, which appear to be less brittle, less limited in their tensile strength, and less subject to time dependent stress failure, make the ceramic materials attractive to the prosthetic dentistry [9].

In this sense, Zirconia is one of the most promising restorative biomaterial, because it has very favorable mechanical and chemical properties suitable for medical application as we presented in **section 1.1.1.3**. Furthermore, it is becoming a prevalent biomaterial in dentistry and dental implantology. It was proved not be cytotoxic and does not enhance the bacterial adhesion, which is lower than on titanium, as demonstrated by both in-vitro and in-vivo studies reported in Ref. [10].

1.1.2. Zirconia-based ceramics

The zirconia-based ceramics (monolithic or composites) are referred commonly as *ZTC* (ZrO_2 Toughened Ceramics). The systems more studied from this family are *classified* in *three*

different categories:

- ***Tetragonal Z*irconia *Polycristals, TZP*:** It is a material composed by almost at 100% tetragonal phase, with a grain size at the range of 0.2-1μm. Generally is stabilized with yttria or ceria oxides and, therefore is denoted with *Y* or *Ce* prefixes respectively and a number that represents the oxide concentration in molar percentage (% mol). For instance, 3Y-TZP represents a tetragonal polycrystalline zirconia stabilized with 3% mol of Y_2O_3. This is the most common TZP material due to its present an interesting mechanical properties; high fracture strength (≈ 1GPa) and moderated fracture toughness (4 - 5MPa√m) [2].

- ***Partially Stabilized Zirconia, PSZ*:** It presents a duplex microstructure; mainly constituted by cubic grains with tetragonal inclusions. The PSZ is obtained by adding high concentrations of stabilizing oxides (8 – 10% mol), generally Magnesium (Mg) or Calcium (Ca) and it is sintered at high temperature (≈ around 1600ºC). The sintering temperature is the main responsible to induce phase transformation and create a composite material with a cubic structure. This phase increases their fracture toughness (≈ 8 - 10MPa√m). On the other hand, produces a reduction of their strength compared to the conventional Y-TZP materials [11].

- ***Dispersed Zirconia Ceramics, DSC*:** It is composed by tetragonal zirconia dispersed particles (5 - 30% in weight) in a ceramic matrix, where the mechanical properties, concretely the fracture toughness, will depend of the transformation of the dispersed zirconia. The most known example of these materials is ZTA (ZrO_2 Toughened Alumina) due to its big commercial development [12].

Along this Bachelor's project, we will focus our attention on TZP materials, mainly 3Y-TZP. This material will be briefly presented in the next section.

1.1.2.1. 3Y-TZP

One of the most used based-zirconia materials is 3Y-TZP (or 3Y-ZrO_2). This material belongs to *TZP* family, and it contains a 3% mol. of Y_2O_3, so it has a high fracture strength as well as high fracture toughness due to it presents a homogeneous monomodal microstructure of tetragonal gains with a maximum grain size of hundreds nanometres. **Figure 1.1.4** exhibits the phase's diagram for the Y-TZP materials. In this diagram is possible to appreciate the different phases, monoclinic, tetragonal and cubic according to the temperatures and the molar

percentage of Y_2O_3. Apart from the mentioned phases, exist another phase called non-transformable tetragonal phase, whose characteristics are an elevated stabilizer proportion in solid solution. This phase is formed by diffuse transformation of cubic ZrO_2 and it has been found in composite ceramic materials with high stabilizer ratio (4 - 5% molar).

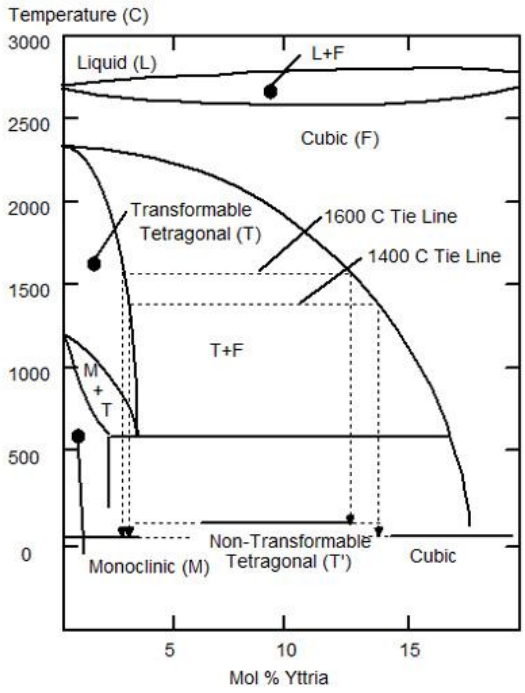

Figure 1.1.4 – *Phase's diagram Y-TZP materials [13].*

Typically the Y-TZP materials contain between 1.75 and 3.5% molar of Y_2O_3. The sintering temperature is ranged between 1400 and 1500ºC, and that allows obtaining fine tetragonal grains with very good mechanical properties. It is necessary to mention that sintering the ceramic specimens at temperatures higher than 1500ºC; the resulting material will present a duplex phase microstructure composed of (tetragonal and cubic grains "*fine*" and "*coarse grains*" respectively).

1.1.3. Cerium oxide, CeO_2

CeO_2 presents a cubic fluorite structure (CaF_2 structure) as it is illustrated in **Figure 1.1.5**. Each Ce atom is surrounded by eight equivalents nearest neighbor O atoms. The O atoms are further surrounded by a tetrahedron of four equivalent Ce atoms [14]. The fluorite structure is relatively open with large octahedral holes and shows large tolerance for atomic disorder mainly attributed to substitution, reduction or oxidation.

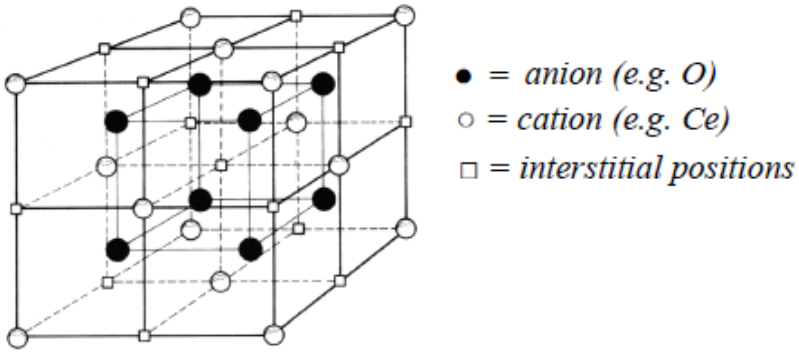

Figure 1.1.5 – *Cubic fluorite structure of CeO_2 [14].*

CeO_2 is pale yellow due to Ce(IV) – O(-II) charge transfer. CeO_2 can be considerably reduced without phase change [15]. The ordering of vacancies in CeO_{2-x} results in a number of phases with $CeO_{1.714}$ as the most reduced phase within the "fluorite-like" region [16]. During reduction to CeO_{2-x}, a color change to blue with minor reduction or to almost black at major reduction occurs [15].

1.1.3.1. Physical properties

The properties of pure ceria are away from the zirconia properties, especially the mechanical properties; some of them are listed in **Table 1.1.2**.

Table 1.1.2 – *Physical properties of CeO_2 [15].*

Physical Properties	Value
Density	7.22 g/cm^3
Hardness	5-6 HV
Bend strength	<100 MPa
Fracture toughness	1.5 MPa√m
Young's modulus	165 GPa
Melting point	2750 K
Thermal conductivity	12 W/mK

1.1.4. ZrO_2-CeO_2 system

ZrO_2-CeO_2 system materials present a big interest as an alternative for ZrO_2-Y_2O_3 materials due to their good mechanical strength and high fracture toughness. On the other hand, the stability region for tetragonal zirconia is wider in ZrO_2- CeO_2 system and the quantity of CeO_2 added

offers the possibility of improves its thermal properties. The partially stabilized zirconia (PSZ) with CeO_2 is considered as an important material in technical applications.

At the same time, doped zirconia with ceria (Ce-TZP) has a higher chemical stabilization and higher fracture toughness (11MPa√m) than Y-TZP, but it has a low mechanical strength. According to the **Figure 1.1.6** which refers to ZrO_2-CeO_2 phase's diagram, the material is completely tetragonal at the most common sintering temperatures (1300 to 1500 ºC), and it converts in metastable, with regard to the monoclinic phase at 400ºC. It is necessary to highlight that this composition is more degradation resistant than the conventional Y-TZP compositions.

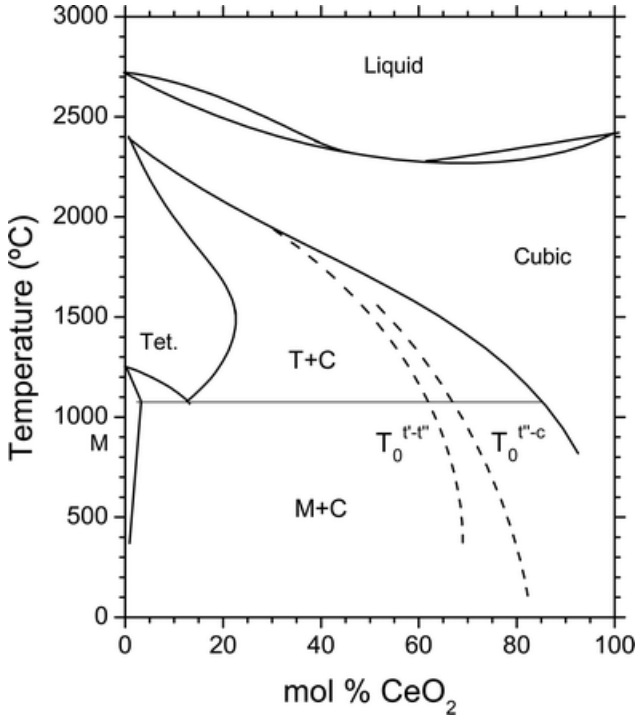

Figure 1.1.6 – *Phase's diagram zirconia-ceria materials [17].*

In order to improve the obtained properties with each stabilizer, several authors have studied the obtained system with the combination of both stabilizers. It has been fabricated (Ce,Y)-TZP ceramics with high bending strength (>800MPa) [18]. The importance of this system is to find the optimum chemical composition, which presents the best properties for each constituent, for example, adding Y_2O_3 improves the mechanical strength of (Ce,Y)-TZP, but the CeO_2 content effect on the mechanical strength depends of the yttria content. For a chemical composition lower than 2% mol of Y_2O_3, add more CeO_2 means an improvement of the mechanical strength, but on the other hand, for higher Y_2O_3 contents and the introduction of more CeO_2 amount, means a reduction of their mechanical strength. However, the hardness and fracture

toughness exhibit an inverse relation for the (Ce,Y)-TZP composite system. The same trend is appreciated in their microstructure; mainly in terms of grain size. In this sense, when the grain size increases, the hardness decreases but the fracture toughness increases as it was found in Ref. [19].

1.2. 3D-printing

Nowadays the rapid prototyping and in particular the 3D -printing technique is becoming more and more important due to its wide range of possibilities.

This technology is based on the addition of material as a superposition of different layers upon one another, in order to create a tridimensional solid product directly from a digital 3D model created through Computer Aided Design (CAD) software.

Printing polymers by using this technique is a widely studied filed, with Fused Deposition Modeling technique, but there are other materials, as ceramics, that can be also 3D-printed with Syringe Extrusion technique. This is not a known field, so talk about 3D-printing with ceramics is still a surprise. Furthermore, ceramic materials have lots of application fields as we already mention in **section 1.1.1.4**. The current techniques for make ceramic crowns as dental prosthesis are slow and difficult. One of the difficulties is to get the real sizes of the tooth, for do that is necessary to subdue the patient to some tests not really pleasant.

With this technique not only is possible to cut the timings, but also is possible to get the same sizes by just doing a radiography and digitalizing it in a computer for take the correct sizes. This is not a much studied field yet.

1.2.1. Fused deposition modeling

Fused Deposition Modeling (*FDM*) is the most popular 3D-printing technique. This technology was patented in 1989 by Scott Crump, who started to commercialize it. This technology allows obtaining products using ABS (acrylonitrile butadiene styrene) or PLA (polyactic acid) polymers. Thanks to this technology the Fused Filament Fabrication (*FFF*) was invented due to the FDM's patent, which protected the FDM's concept, so a similar technology had to be created. The machine used in this Bachelor's project, presented in **section 3.2**, uses this technique for 3D-printing with polymers; see **Figure 1.2.1** [20].

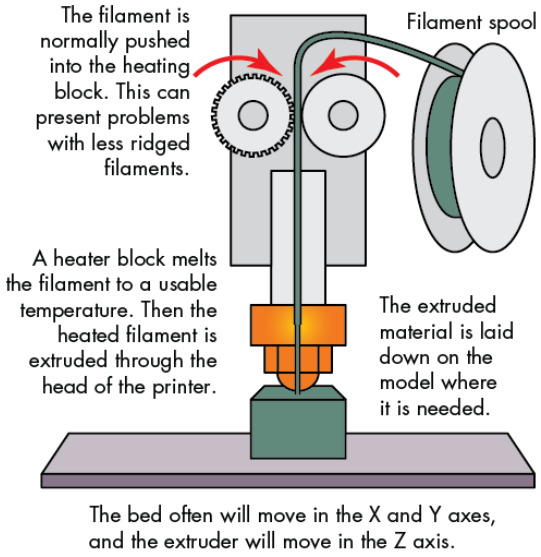

Figure 1.2.1 – *Fusion Filament Fabrication procedure [21].*

1.2.2. Syringe extrusion

This method consists of an extruder that is a combination of an infilled syringe with the printable material and nozzle with a determined section shape. Applying pressure on the top pd the syringe it is possible to extrude the printable material in the form of filaments, with a section determined by the nozzle shape. The printing process to conform the layers using these extruded filaments is the same as the utilized for the *FFF* technique [22].

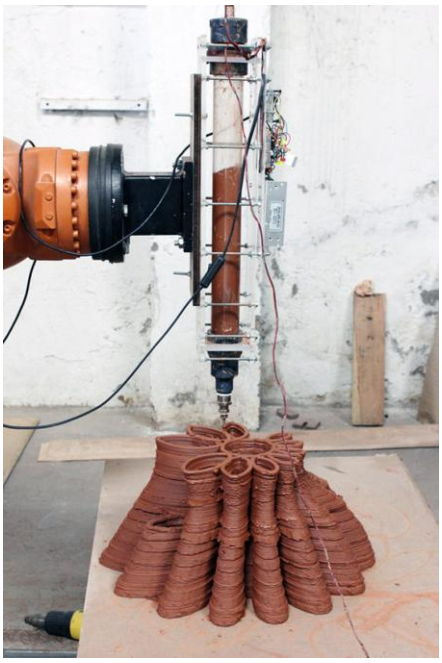

Figure 1.2.2 – *Syringe extrusion procedure [23].*

1.3. State of the art

Hundreds of manuscripts related to study the microstructure, mechanical properties as well as their transformability have been published along the last decades for zirconia based ceramic materials. However, scarce information is available in the literature for advance ceramic samples performed by the rapid prototyping technique.

The 3D-printing technique was originated to be used to print polymer materials. Recently, this technology has been started to be employed to develop ceramic systems with complex shapes. However, this technique is still under research due to the complexity to well understand some rheologycal aspects during the production and printing of ceramic pastes, which is one of the main key parameters for this technique. For these reasons, this technology has not been applied to the industrial production because exist a lot of uncertainties and printing defect (i.e. high porosity, etc.) that are necessary to be solve. It does not mean that this process is dismissed for ceramic pieces fabrication, due to it presents several advantages compared to the traditional process: low prices, allows develop complex shapes, quickly and final pieces with low densities. However, until now, scarce information related to print advance ceramic materials based zirconia as well as the correct way to determine their mechanical response is available in the literature.

Along this section, some recent articles will be summarized in order to give a general overview about what it is possible to find in the literature related to this technique priting advanced ceramic materials.

The first article was published in 2008 called "*A review of process development steps for new material systems in three Dimensional Printing (3DP)"* [24]. The authors expose that 3D-printing is a technique that allows creating infinity and complex geometries. That is thanks to use polymeric binders in the printer solutions. This technique allows creating impossible forms by increasing the fabrication process speed. In this article the authors highlight the importance of the post-impression process.

In 2009 another manuscript called *"Direct Inkjet Printing of Dental Prostheses Made of Zirconia*" was published [25]. In this article the authors discuss the main advantages to print zirconia based dental prosthesis. Following the document, the CAD/CAM techniques aren't as precise as printing techniques. But printing methods can cause micro-cracks into the final material. One of the main problems is found in the post-processing process, while the samples

lose humidity. This effect generates micro-cracks.

Related to the 3D design made type, the article “High-strength cellular ceramic composites with 3D microarchitecture” [26], which was published in 2014, shows the mechanical and structural properties of different types of 3D printed ceramic microarchitectures.

Another recently article published in 2015 and entitled “*Analysis of the mechanical response of bio mimetic materials with highly oriented microstructures through 3D-printing, mechanical testing and modelling*” [27]; the microstructure orientation for 3D-printed Chiton specimenswas investigated. During the same year, a manuscript entitled *“Extrusion-based 3D Printing of ceramic components”* [28] was also published, showing how important is the engineering connected to ceramics in the current industry. The authors forecast that the use of ceramic materials will increase during the next years and will play an important role for biomedical applications. This 3D-printing technique allows decreasing the fabrication process costs, offering largest complexity, obtaining personalized pieces and getting a better production control. All this has been possible developing ceramic pastes with polymeric binders in order to develop printable hydrogels.

How it can be observed, the publication dates related to this topic ranges between the last 20 years, which demonstrates one more time that this topic, is quite new for an industrial application. Another important thing that all this papers have in common is that most of them talk about zirconia as a material for print and use in dentistry as a biomedical material, highlighting that this technique is suitable to print complex geometries.

2. Objectives

For all the reasons previously mentioned in the introduction part the following goals can be drawn:

i) To 3D-print cube of zirconia doped with different ceria contents.

ii) To evaluate the microstructural parameters (density, porosity, roughness and grain size) at different sintering temperatures (1450 and 1740ºC).

iii) To evaluate the mechanical behaviour (Vicker's hardness and spherical cyclic tests) for those printed materials as a function of their sintering temperature at room conditions and under simulated body fluid.

iv) To evaluate some optical parameters by using UV-visible spectroscopy as a function of the sintering temperature and chemical composition in terms of Ce.

3. Experimental methods

The first part of this section describes the methodology employed to prepare the material and the different ceramic pastes used along this Bachelor's project, as well as the samples preparation process in terms to reduce the superficial roughness to get a suitable surface to investigate their mechanical properties. Secondly part of this chapter presents the procedure employed to determine some microstructural parameters (e.g. density, porosity, grain size, etc.); after that the mechanical proprieties (e.g. Vicker's hardness, Herzian cyclic tests "at room and under water conditions") and finally the evaluation of their optical properties by using UV-visible Spectrophotometer.

3.1. Material

The materials used to develop different ceramic composite materials by using the rapid prototyping technique were: zirconia stabilized with a 3% mol of Y_2O_3 (3Y-ZrO_2 or 3Y-TZP) and ceria (CeO_2) as the main ceramic materials and agar-agar as a gelling agent.

3.1.1. Material's preparation

The gelling material employed was obtained after more than thirty trials, getting the best paste with the following composition: 15g of ceramic powder, 50 ml of distilled water and 0.7g of "*Agar-Agar*".

As it has been mentioned before, four different ceramic samples were printed and investigated with different ceramic content, see **Table 3.1.1.**

Table 3.1.1 – *Sample's content.*

	Sample 1	**Sample 2**	**Sample 3**	**Sample 4**
Distilled water (mg)	50	50	50	50
3Y-TZP (%)	95	90	80	50
CeO_2 (%)	5	10	20	50
3Y-TZP (mg)	14.25	13.5	12.0	7.5
CeO_2 (mg)	0.75	1.5	3.0	7.5
Agar-Agar (mg)	0.7	0.7	0.7	0.7

The four ceramic pastes have been prepared following the next steps:

i) **Weight and mix the ceramic powders and the solvent agent** in a 250 ml glass container each component present in **Table 3.1.1**. After that, in order to get an homogeneous mixture, the components may be ultrasonically mixture during 2 min. by using the Omni Ruptor 4000 equipment with an output frequency of 40Hz. This equipment helps homogenize the mixture as well as reduce the ceramic agglomerate particles.

ii) After that, the ceramic dissolution may be **heated until** reach a temperature of around **90ºC** by using the system presented in this **Figure 3.1.1**. The set-up presented in this figure consists of: a heating magnetic stirrer (Velp-Scientifica model) coupled with a thermometer, recipient with water and the pliers. When the solution reached the desired temperature, around 90ºC, the gelling agent is added[1]. During the addition of the gelling agent, the temperature slightly drops.

iii) Then, when the dissolution reaches again the desired temperature of around 90ºC, it is necessary to increase the mixture speed until 200 rpm in order to homogenise the final paste.

Figure 3.1.1 – *Heating set-up.*

iv) After 2 minutes, it is necessary to remove the cooler system, the magnet and subsequently apply ultrasounds for extra 2 more min.

[1] It is necessary to mention that along the entire, the solution should be stirring constantly in order to avoid that the ceramic and gelling elements will precipitate. To avoid the water evaporation we recommend putting a glass with cold water as a cover for the beaker (see **Figure 3.1.1**, right hand side).

v) Then, ultrasound the final mixture and mix again increasing the revolutions to 600 rpm. After 5 min, apply again ultrasounds for 2 more min. This process will avoid that the gelling agent will precipitate during the cooling process. At least, for the final solution to be moulded as it is depicted in **Figure 3.1.2**, let decrease the temperature until reach the desired texture.

Figure 3.1.2 – *Final solution's cooling in a mould (right hand side) and after demoulding (left hand side).*

3.2. 3D-Printing technique

This section will explain with details the different steps followed to get a final 3D-printed specimens with the following dimensions; 20x20x6 mm.

The 3D-printer used during this Bachelor's project has been a BCN3D + Dual Paste (see **Figure 3.2.1**) made by Centre CIM-UPC foundation. This printer consists of 2 extruders which can move along *x* and *z* axis and 1 base which allow movements along *y* axis. . In order to control the machine the device has a little screen and a button. By using this button is possible to choose the desired option as well as select the proper option desired to use.

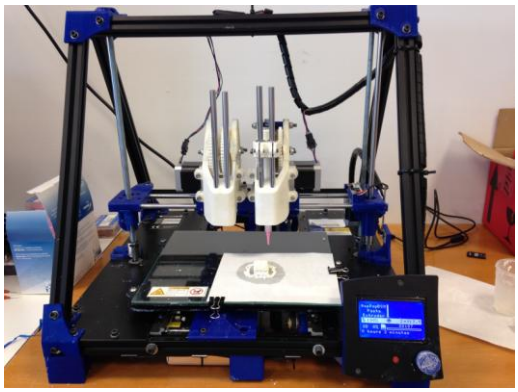

Figure 3.2.1 – *General set-up for theBCN3D + Dual Paste.*

3.2.1. 3D file development

The desired ceramic specimen may be 3D-develop by using a special software and afterwards convert the code in order the printer will be able to read the printing code. To make this file 2 different steps have been followed:

i) Creation of the desired shape in a CAD file, and

ii) Transformation to a G-code file with Slic3r software.

3.2.1.1. Figure creation in a CAD file

The first step to obtain the final file to print with the equipment presented above (see **Figure 3.2.1**), it is necessary to create the desired figure in a CAD file. Initially, SolidWorks® software has been used to create a 20x20x6 mm cube. In order to create the figure is necessary to keep in mind that the height of the figure has to be a multiple number of the extruder's diameter which is 1.5 mm what means that the cube performed in this Bachelor's project is made by four layers. Once the figure is created is necessary to save it in .STL format.

After that, it is necessary to locate the specimen on the correct axis by using the Netfabb Basic 5.2 software, as it clearly shows in **Figure 3.2.2**. By using this software, two different actions may be done at the same time:

i) The first one is to locate the figure on the correct position as in **Figure 3.2.3**. For this action is necessary to use the buttons *Move* and *Rotate parts* as it is shown in **Figure 3.2.4**.

ii) The second action is to repair the structure by clicking on the *Repair button* (see **Figure 3.2.5**) this action allows the closure of the piece's triangles and avoids future conflicts with the codification for print. So the steps for the repair are click on the *Repair button* → *Automatic repair* → *Apply repair*.

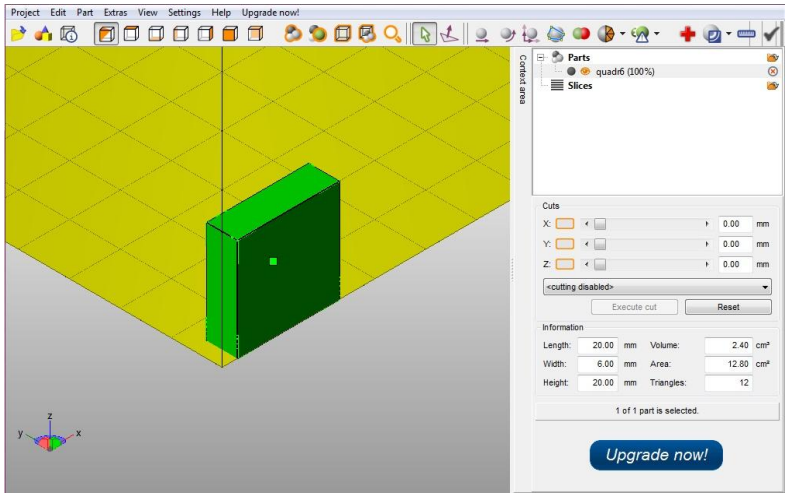

Figure 3.2.2 – *Netfabb Basic 5.2.*

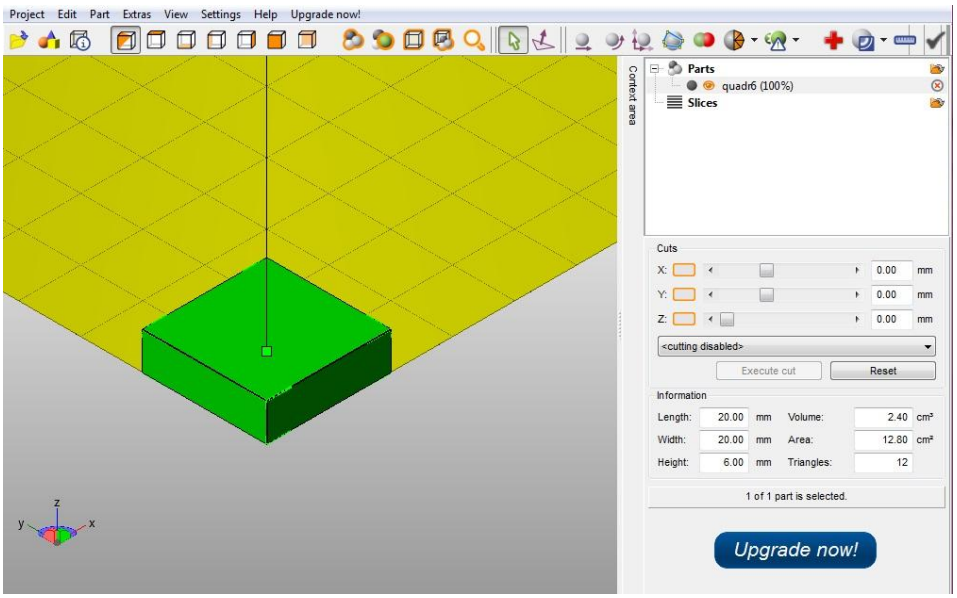

Figure 3.2.3 – *Correct position on axis.*

Figure 3.2.4 – *Move and Rotate parts buttons.*

Figure 3.2.5 – *Repair button.*

Finally, it is necessary to save the figure repaired clicking *Part → Export Part → as STL*.

3.2.1.2. Transformation to G-code and printer parameters

In order to convert the original code into a printable code, the Slic3r software has been

employed, see **Figure 3.2.6**. By using this software, it helps to transform the **.STL files** to **G-code**. It is necessary to mention, that by using the Slic3r software is possible to define the main printing parameter (e.g. speeds, layer heights, among others).

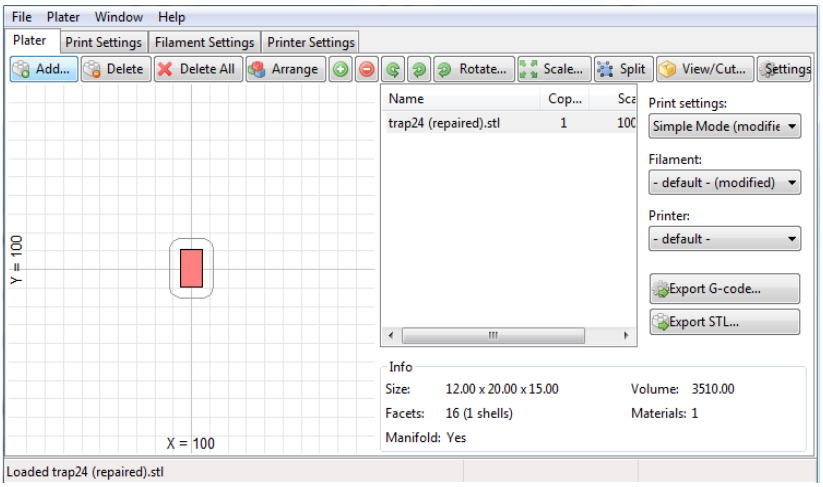

Figure 3.2.6 – *Slic3r general view.*

Initially, it is necessary to work in expert mode (*File → Preferences → Mode expert*). Once we are in expert mode is possible to change the printer settings. In this case the <u>printer settings</u> that have to take into account are:

- **Layer and perimeter:** Layer height and the first layer height make reference to the nozzle's diameter, which in our case both present the same value and equals to 1.5mm (see **Figure 3.2.7**).

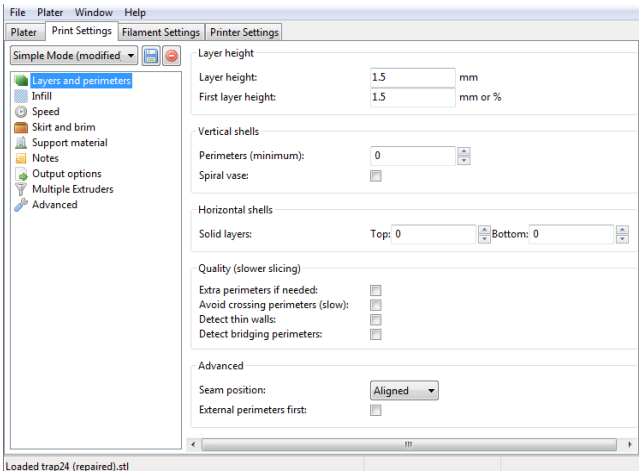

Figure 3.2.7 – *Layers and perimeters.*

- **Infill:** Along this project, the fill density parameter has been kept constant and equals to 100% (in order to reach dense materials, the distance between two consecutive lines of printing may be the minimum possible, see **Figure 3.2.8**). The fill pattern (see **Figure 3.2.9**), as well as the top/bottom fill pattern need to be rectilinear to get the correct printed direction for this Bachelor's project.

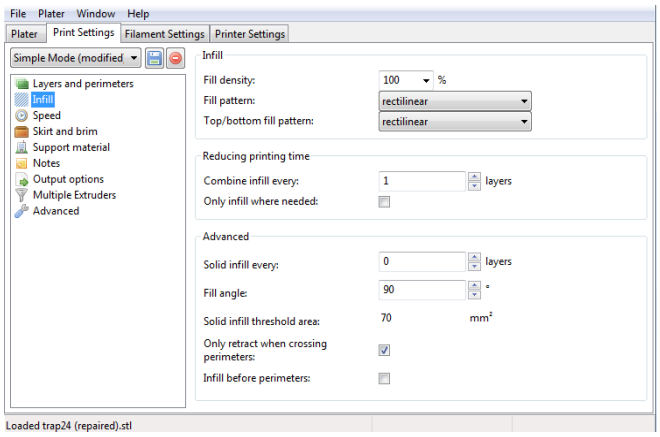

Figure 3.2.8 – *Fill pattern.*

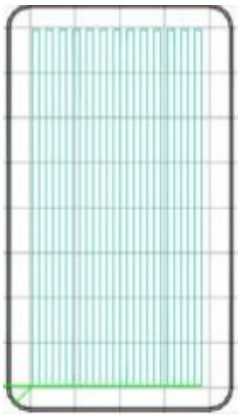

Figure 3.2.9 – *Infill.*

- **Speed**: After different trials it has decided that the speed parameters that better works for this ceramic system is summarized in **Table 3.2.1** and presented in **Figure 3.2.10**.

Table 3.2.1 – *Speed parameters.*

Parameter	Value
External perimeters (%)	100
Infill (mm/s)	8
Solid infill (mm/s)	10
Top solid infill (mm/s)	8
Support material (mm/s)	10
Support material interface (%)	100
Travel	20
First layer speed (%)	100

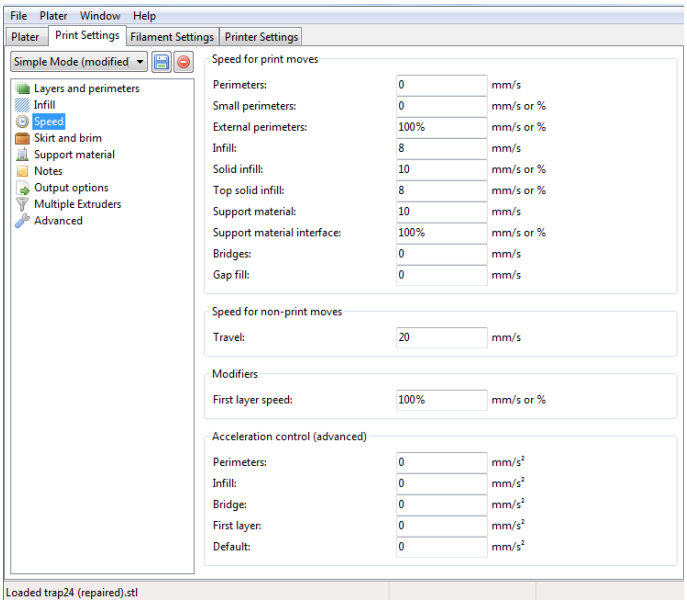

Figure 3.2.10 – *Speed.*

- **Skirt and brim:** These parameters make reference to the extruded paste before the printing process. This first extrusion is made to secure the good fluidity of the paste and to eliminate the remaining air bubbles and/or the excess of water. In this case it has been decided to make one loop with a distance from the object of a 6 mm, with one layer of skirt height and with 0 mm minimum extrusion length as it is depicted in **Figure 3.2.11**. The other parameters presented in this folder are: distance from object, skirt height, minimum extrusion length, etc. All of them do not affect the printing process of ceramic composite materials.

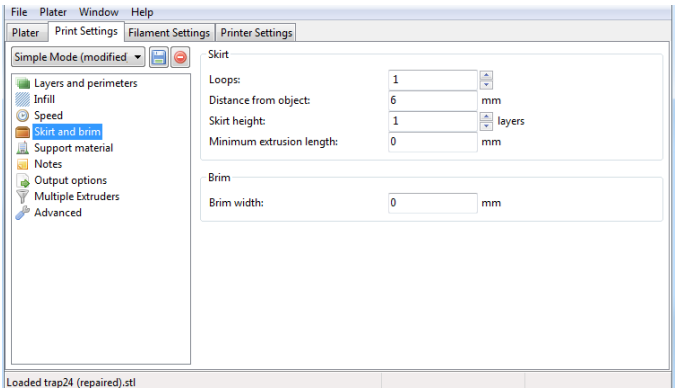

Figure 3.2.11 – *Skirt and Birm.*

Furthermore, the support material, note, output options, multiple extruders and advanced, parameters will not be used, for that reason is not necessary to configure any other parameter.

Afterwards, it is necessary to define the filament settings. Mainly, these settings were developed to define the parameters to print polymeric components. However, for ceramic materials it is necessary to introduce slightly modifications into the appropriate parameters. These will be presented and briefly explained below:

- **Filament**: One of the most important settings to define the correct filament parameters is the interior diameter of the syringe, which in our particular case is around 8.6 mm. The extrusion multiplier parameter change the extruder flux proportion, it will be 1 for all ceramic cases as it is depicted in **Figure 3.2.12**. Temperature parameters will be 0 due to this option is not used for ceramic materials due to in this case we use a gelling agent in order to create ceramic-polymeric materials to maintain the desired structure during the printing process.

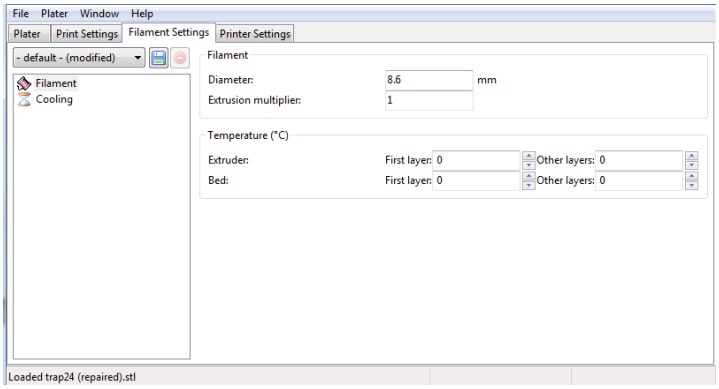

Figure 3.2.12 – *Filament.*

- **Cooling**: These parameters will be the default ones because cooling refers to different ceiling fans that this printer does not have, they are only for plastic 3D-printers.

The main settings to take into account and modify are listed below:

- **General:** The size and coordinate parameters allow defining the exactly size of the bed and the print centre to decide where the printer should start to print. RepRap (Marlin/Sprinter/Repetier) needs to be selected on G-code flavour parameter. Regarding to the extruders parameter for this work has to be just 1. All the other parameters are not necessary to be modified due to they do not are required to print ceramic pastes, see **Figure 3.2.13**.

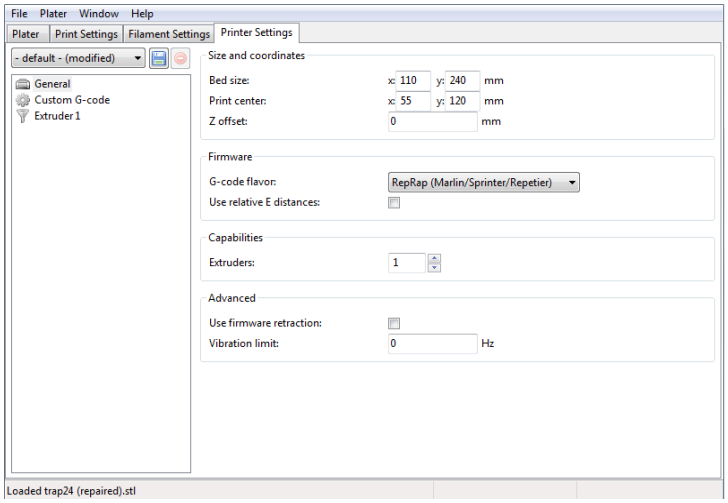

Figure 3.2.13 – *General.*

- **Custom G-code:** Noozle diameter refers to the real nozzle diameter. The retraction section only works for plastic printing so these parameters need to be deactivated as defined in **Figure 3.2.14**.

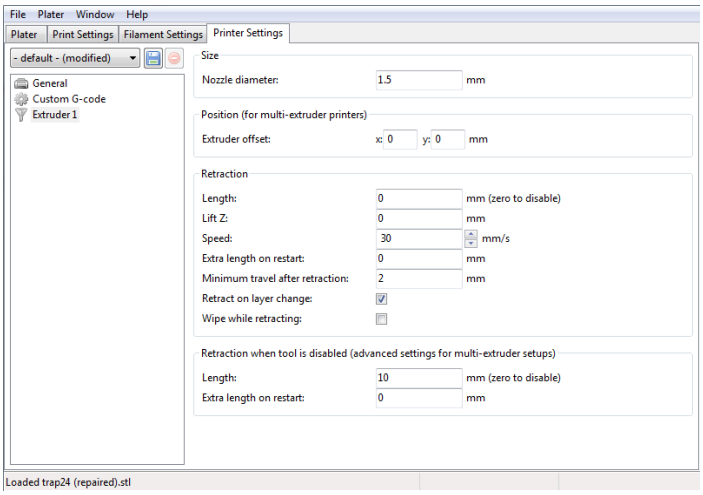

Figure 3.2.14 – *Custom G-code.*

After all these steps, it is necessary to return to *Plater* icon and select *Export G-code*, **Figure 3.2.15**. This file has to be stored in a SD card.

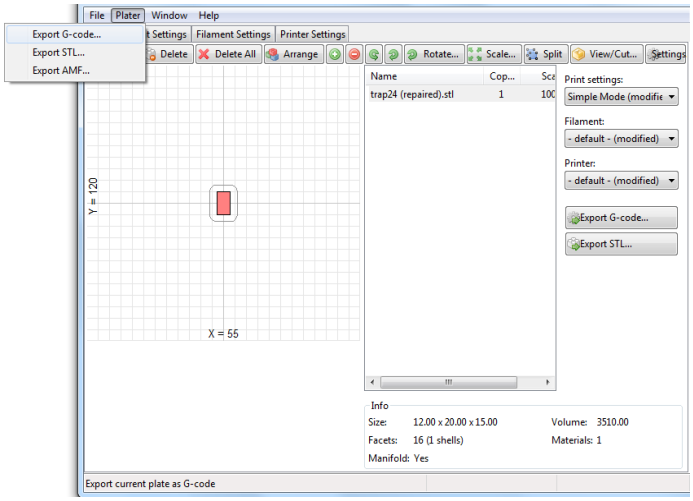

Figure 3.2.15 – *Export G-code.*

3.2.2. Printer preparation

The last step before begin to print will be briefly explained in this section. First of all, it is necessary to turn ON the 3D-printing button machine, see **Figure 3.2.16**. The printer will turn on and afterwards we will use the blue bottom to move between the different options (see red arrow in **Figure 3.2.17**).

Figure 3.2.16 – *Turn ON button.*

Figure 3.2.17 – *3D-printer screen.*

The different actions required to use the 3D-printing are presented below:

- ***Prepare > Move Axis > Move 0.1mm > Extruder Right*****:** this action allows the gears movement of the extruder rotating the blue bottom to the left for introduce the syringe into its correct place or for remove it rotating the bottom to the right.

- ***Prepare > Extruder DUPLICATION*:** this action should be enabled to avoid future problems about choosing the correct extruder for printing. For this particular Bachelor's project, both extruders will not be used at the same time, so enabling the extruder duplication the two extruders will print the same but just one will have the syringe for print.

3.2.3. Syringe preparation

This step is one of the most important steps to obtain a good printed specimen. It depends of that process that we acquire a homogeneous printing without air bubbles between the different printing filaments or between layers.

To obtain a good syringe filling is important follow the next steps:

1. First of all is necessary to chop the final material that we had obtained at the materials preparation part and explained in detail in **section 3.1.1**, into small pieces and afterwards with the aid of a pestle and mortar reduce the size of the pieces until it seems a homogeneous solution. To secure that the solution is homogeneous the last thing we need to do is to put the solution between two glasses and make pressure for mash the final mass, see **Figure 3.2.18**.

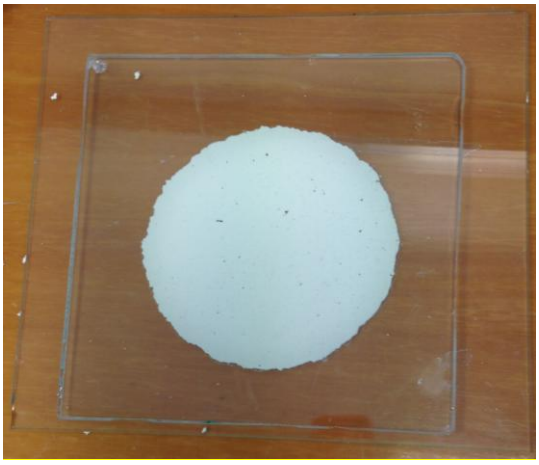

Figure 3.2.18 – *Final mass mashed with two glasses.*

2. Once the mass is mashed and ready to be used is necessary to introduce it in the syringe, for that we used a spatula and a plastic bag, **Figure 3.2.19**. With the help of the spatula the mass is picked up of the glass and introduced into the plastic bag. When all the mass is inside the plastic bag one of the bottom corners has to be cut as is depicted in **Figure 3.2.20**, simulating a pastry bag.

Figure 3.2.19 – *Material used.*

Figure 3.2.20 – *Cut corner.*

3. When our hand-made pastry bag is ready is time to fill the syringe, with this technique is less than 5 seconds to fill the syringe meanwhile with other traditional methods is more than 2 min.

4. After filling the syringe is important not to forget to put the piston at the top of the syringe, to avoid missing material during the printing process.

3.2.4. Printing

Once the syringe is prepared, the printing process is ready to 3D-print ceramic cube materials. For introduce the syringe and the plunger into the printer we will use the action *Move Axis*, see **section 3.2.2**. The plunger will be introduced until the ceramic paste and ejected throw the nozzle.

To print the desired cube for a specific ceramic paste is necessary to introduce de SD card into the printer and use the action ***Print from SD > cube.gcode*** using the blue bottom previously explained in **section 3.2.2**. The printer will start to move and the cube will start to be printed, **Figure 3.2.21**. After 1 min approx the cube is printed, **Figure 3.2.22**.

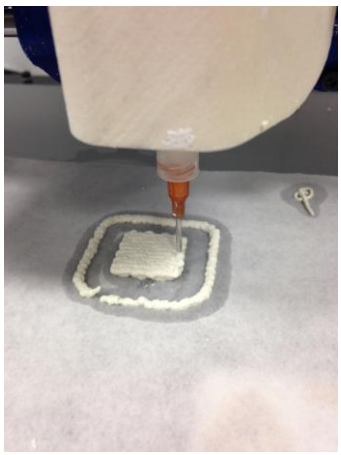

Figure 3.2.21 – *Printing process.*

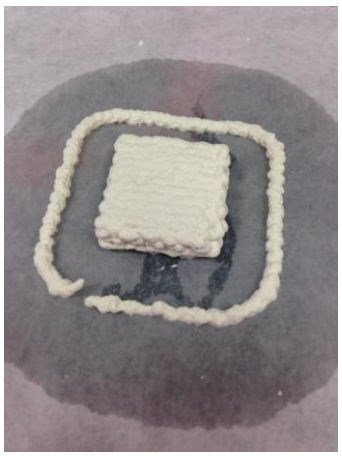

Figure 3.2.22 – *Printed cube.*

3.3. Samples preparation

After the 3D-printing process, the green ceramic specimens is necessary to let it dry during two or three days before continue with the sintering process, if not all the water inside the cube will try to leave it too quick and will deform the cube as an explosion; obtaining a final specimen with a lot of residual cracks.

3.3.1. Sintering process

After that, the specimens were sintered at two different temperatures, 1450 and 1740ºC, due to the nature of the raw ceramic materials need different temperatures to reach a desired density. The raw materials employed here, 3Y-TZP and CeO_2, present different sintering temperatures. So for this reason it has decided to sinter the different investigated materials at two different temperatures, one at 1450ºC, in order to lead sinter the 3Y-TZP without modify the tetragonal structure [29], while the other temperature around 1740ºC, in order to help to improve the CeO_2 material sintering. However, at this temperature, the tetragonal phase for the 3Y-TZP transforms to cubic phase. **Table 3.3.1** summarizes the main parameters for all the specimens investigated along this Bachelor's project.

Table 3.3.1 – *Sample's composition and sintering temperature.*

	Ceramic elements (%)		**Sintering Temperature (ºC)**	**Label**
	3Y-TZP	**CeO_2**		
Sample 1.1	95	5	1450	95_1450
Sample 1.2	95	5	1740	95_1740
Sample 2.1	90	10	1450	90_1450
Sample 2.2	90	10	1740	90_1740
Sample 3.1	80	20	1450	80_1450
Sample 3.2	80	20	1740	80_1740
Sample 4.1	50	50	1450	50_1450
Sample 4.2	50	50	1740	50_1740

Sintering process has been conducted in a Nabartherm furnace (see **Figure 3.3.1**). For the sintering temperature of 1450ºC, it has been necessary eight hours to reach the desired temperature, so the heating rate temperature for has been held constant and equals to

3ºC/min, after reaching, the desired temperature, it was keep constant during one hour and subsequently cooled until room temperature with the same speed rate. The same heating and cooling process for the specimen sintered at 1740ºC was done following with the same thermic cycle with a heating and cooling constant rate of 3.5ºC/min.

Figure 3.3.1 – *Nabertherm sintering furnace.*

3.3.2. Polishing process

After sintering process, the specimens have to be prepared in order to get a suitable surface to investigate the main microstructural and mechanical parameters. For that, the specimens have been conventionally polished following the protocol described below.

Five different polishing discs from Struers with different grain size have been used to polish the desired specimens by using the polishing machine presented in **Figure 3.3.2**. The polishing process has been conducted at a constant polishing speed of around 150 rpm.

The **polishing process steps** are summarized below:

1. Roughing process to obtain a flat surface by using a P320 disc and using tape water as a lubricant and during the necessary time to reach a flat sourface.

2. P600/1200 disc with tape water as a lubricant during 10 min.

3. MD-Plan disc with a diamond slurry suspension of 30μm during 15 min.

4. MD-Dac disc with a diamond slurry suspension of 6μm during 15 min.

5. MD-Dac disc with a diamond slurry suspension of 3μm during 15 min.

6. MD-Nap disc with colloidal silica as a lubricant during 20 min.

Figure 3.3.2 – *Polishing machine.*

3.4. Samples characterization

3.4.1. Grain size

Finally, in order to better understand the microstructural parameter for 3D printed specimens, the grain size has been studied for a sample with a ceria content of around 5 wt. % sintered at 1450 and 1740ºC. The thermal treatment to reveal the grain size has been conducted during 1 h at a temperature of around 100ºC below the sintering temperature; 1350 and 1640ºC, respectively.

After that, the specimens were mounted in an aluminum stub and covered with carbon in order to observe the microstructure by using a field emission scanning electron microscopy. Five different samples have been taken per each temperature and the linear intercept method has been used in order to determine the grain size per each specimen.

3.4.2. Density by Archimedes

When the samples are sintered, and before the polishing process, is possible to calculate the density of each one by using the Archimedes method. For that process a PB303 DeltaRange®

(Mettler-Toledo), presented in **Figure 3.4.1** has been used, with a precision scale of a 0.01mg. The system employed and presented in this figure contains a beaker with water and a wire structure composed by two containers, one on the top, where the specimen will be placed (see red arrow in **Figure 3.4.1**) and measure the real weigh of the sample in air and the second container which is submerged into distilled water. With that second container, the volume for the displaced water when the sample is inside will be measured. Then, the density can be determined as the quotient between these two measures as present in **equation 3.4.1**.

$$\rho = \frac{m}{V} \qquad (3.4.1)$$

Figure 3.4.1 – *Precision scale.*

3.4.3. Surface topography

3.4.3.1. Roughness analysis by using the profilometry technique

Roughness term is called the set of surface irregularities due to the machining process [30], to define the surface roughness is necessary to know the two important parameters described below:

- **R_a:** The Roughness Average (R_a) is the most commonly used parameter for expressing measurements of surface contour. The value represents the arithmetic average of the height of the roughness irregularities above the mean line along a sampling length [31].

- **R_q:** Geometric Avarage Roughness, R_q, is the current term for what was formerly called root-mean-square or RMS. R_q is the geometric average height of roughness-component irregularities from the mean line measured within a sampling length [32].

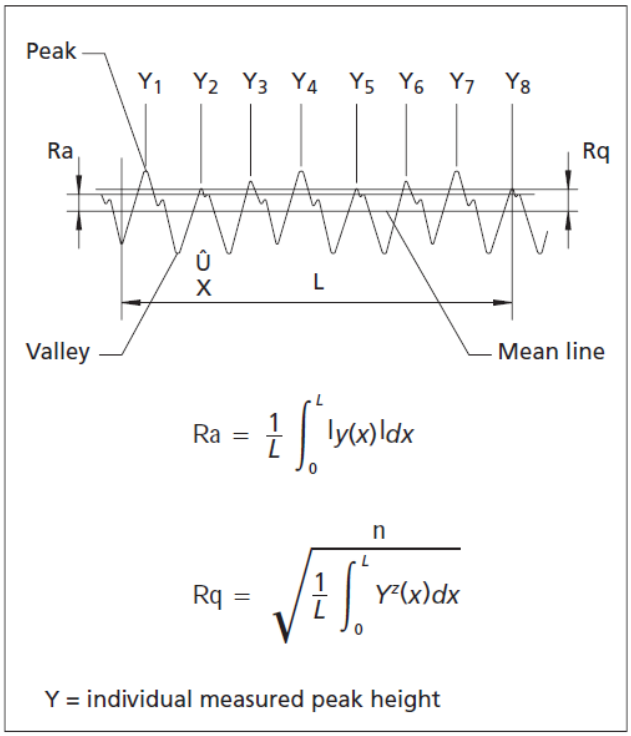

Figure 3.4.2 – *R_a and R_q representation [31].*

There are two other parameters that have been taken to define the surface topography:

- **R_t:** Maximum Height of the Profile (R_t) is the maximum peak-to-valley height in the sampling length.
- **R_z:** Mean roughness Depth (R_z) is the arithmetic mean value of the single roughness depths of consecutive sampling lengths.

Profilometry is a technique that characterizes the surface to obtain measurements of roughness. To study the surface roughness of the 3D-printed specimens, a profilometer was used. A profilometer functions by dragging horizontally (x) a diamond tip (radius of 12.5 µm) across the surface and measuring the vertical (y) displacement, having a constant load of 3 mg. This way a profile is obtained, thanks to which it is possible to measure statistically meaningful values such as R_a and R_q.

A Map Scan of 2x0.5mm has been done in order to characterize the roughness for the 3D-printed specimens by using the Dektak® 150 profiler from Veeco, see **Figure 3.4.3**:

This technique measures the vertical displacement with a diamond tip across the surface. The result give information about several roughness parameters, but the most important roughness parameters are: R_a, and R_q both of them have been defined by doing the arithmetic mean of 10 measures of each sample.

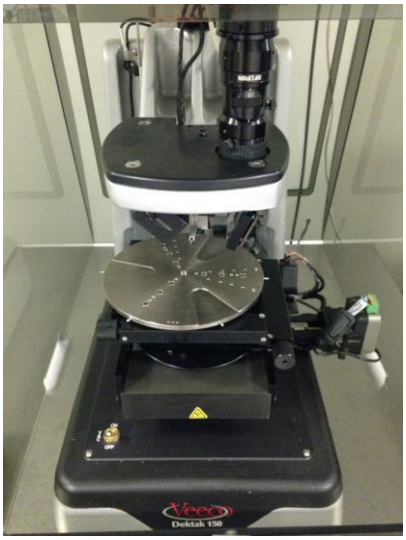

Figure 3.4.3 – *Dektak Profilometer.*

3.4.3.2. Laser Scanning Confocal microscope

A scanning type laser microscope aims a laser beam at a very small spot through objective lens and scans over the specimen in *X-Y* directions. It then captures light from the specimen with the detector and outputs the image of the specimen onto the monitor, see **Figure 3.4.4**.

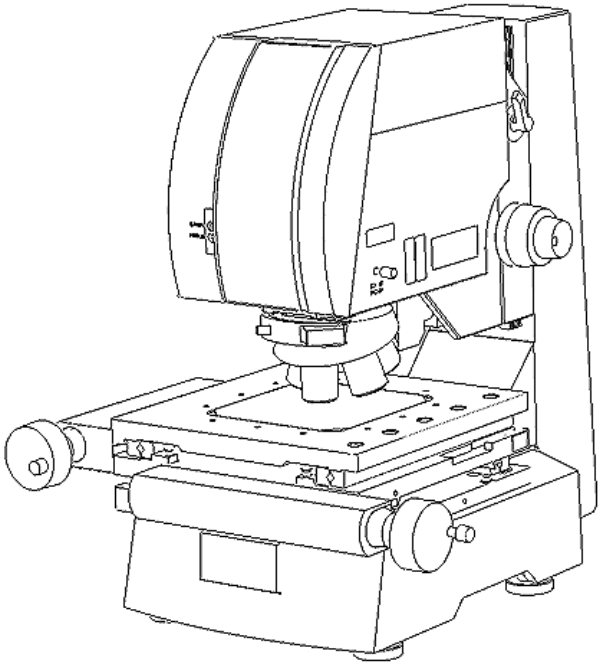

Figure 3.4.4 – *Confocal microscope.*

To correctly define the microstructure in terms of porosity for the 3D-ceramic printing samples a laser scanning confocal microscope (LSCM) has been used for this pourpose. It has been useful for describe the surface by 2D and 3D pictures to define the profile.

The confocal microscope is a laser microscope which is composed by two diaphragms, one of illumination and one of detection. The detection one removes the light coming from the mayor and bottom plans, that allows for get a better resolution of the picture. The main quality of this microscope is to obtain totally well focused pictures thanks to the overlapping of the different captured pictures. Besides the fact that with this confocal microscope is possible to get material surface 3D pictures, which are so useful for define the samples.

The microscope used has been an OLYMPUS LEXT model. This microscope brings in one analysis software which allows to analyze the pictures applying different filter to differentiate the pores than the material for example or which is possible to correct the angle or to change the contrast. With that analysis software the percentage of the porosity has been measured. Due to the size of the pores the recommended magnifications for work are between 5 and 10X, so in this case the measurements have done with a 5X magnifications and with a zoom of 1.4 making a total of 7X magnifications.

3.4.4. Porosity

The porosity analysis has been conducted by using a total amount of four LSCM images as well as using the Image J software. One for characterize the medium pore size of each sample and the second for characterize the porosity percentage. Both of them have been done with the LSCM equipment presented above (see **section 3.4.2**).

The measurement of the medium pore size it has used different picture analysis software, for this case it has been decided to use Image J. This software allows getting measures from a firstly defined scale, so first of all is necessary to define the scale giving to the software a known measure by calibrating the image by using the proper scale presented in the bottom part of the **Figure 3.4.5**. Once the scale is defined is possible to take the pertinent measures. It has been measured at least 10 pores per sample and it has been taken 4 measures per pore in order to have statistical signification.

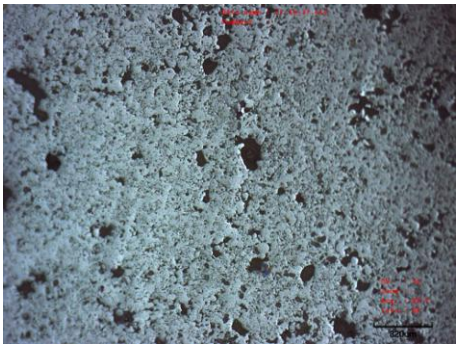

Figure 3.4.5 *– Scale at the right's bottom.*

3.4.5. Ultraviolet (UV) visible Spectrometry: Optical properties

By "optical property" is meant a material's response to exposure to electromagnetic radiation and, in particular, to visible light. By using this technique, three different optical properties have been evaluated: reflectance (*R*), transmittance (*T*) and absorbance (*A*). All of these parameters can be determined by using **equation 3.4.2**. So to know all of them, reflectance and transmittance have been measured and absorbance has been calculated following the **equation 3.4.2**.

$$R + T + A = 1 \qquad (3.4.2)$$

For the measure of these properties it has been used a UV-visible spectrophotometer model UV-3600 from Shimadzu®, see **Figure 3.4.6**.

Figure 3.4.6 – *UV-3600 Spectrophotometer.*

The spectrophotometer employed in this Bachelor's project is a spectrophotometer able to throw light beams from the ultraviolet to the visible and infrared. Thanks to this property it is possible to know the reflectance (*R*), the transmittance (*T*) and the absorbance (*A*) at the visible and at the ultraviolet. According to the property desired to determine is necessary to place the sample at the right position, for measure reflectance the sample has to be in position 1 of the representation depicted in **Figure 3.4.7**, and for measure transmittance the sample needs to be in position 2 of the same image.

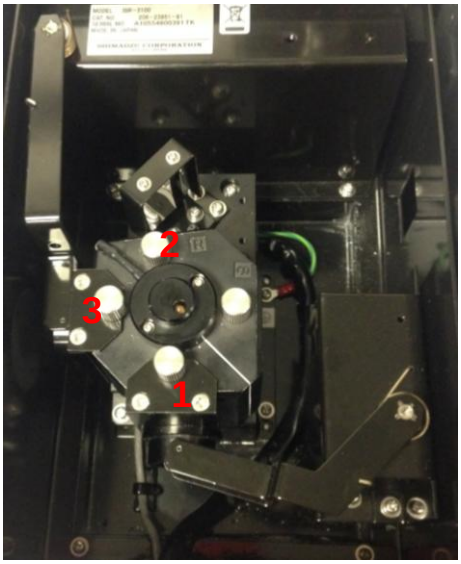

Figure 3.4.7 – *Measurement positions for the UV-3600 spectrophotometer.*

All the measurements have done in 2D, with a slit width of 5.0 and with a wave length ranged between 250 and 2000 nm at intervals of 5 nm, in order to get the response from the UV to the infrared and to see how it works on the infrared.

3.4.5.1. Reflectance

Reflectance refers to the capacity of a body to reflect the light.

When we talk about rough surfaces it is necessary to differentiate between specular and diffuse reflectance, see **Figure 3.4.9**. The sum of these two is the total reflectance.

The light that reflects at the same angle, but opposite, to the light source is called specular reflected light. This specular component reflects as it was a mirror. On the other hand, the light that is not specullary reflected and it is scattered in a lot of directions is called diffuse reflectance. Both reflections are presented in **Figure 3.4.8** [33].

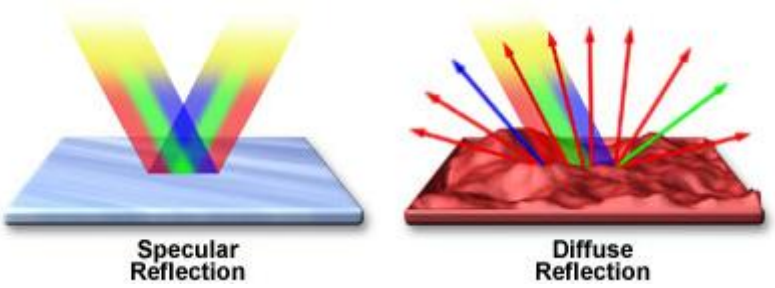

Figure 3.4.8 – *Specular and Diffuse reflection [33].*

For the measurement of the reflectance is necessary to do a baseline before every different sample measurement, which consist in measure the reflectance of a barium sulfate ($BaSO_4$) sample having as a base another $BaSO_4$, as in **Figure 3.4.9**, placing the two samples in places 1 and 3 of **Figure 3.4.7**. Once the baseline is done it is possible to measure the reflectance of a sample by placing our sample in position 1, and one sample of $BaSO_4$ in position 3 of the **Figure 3.4.7**. After that, the test can be done by clicking start. The result is a percentage of the total reflection per wave length.

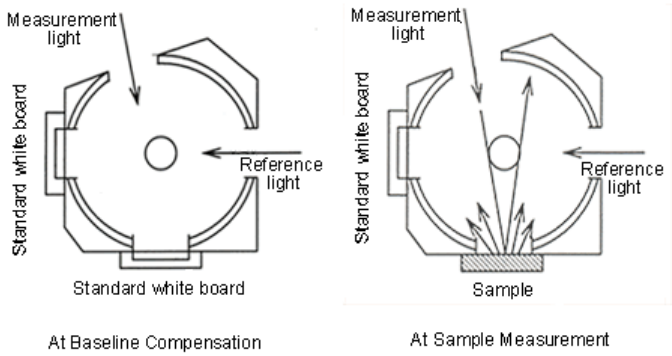

Figure 3.4.9 – *Schematic representations of diffuse reflection including specular reflection [34].*

3.4.5.2. Transmittance

Transmittance is the amount of flux transmitted by a surface, normalized by the amount of incident flux on it, see **Figure 3.4.10**.

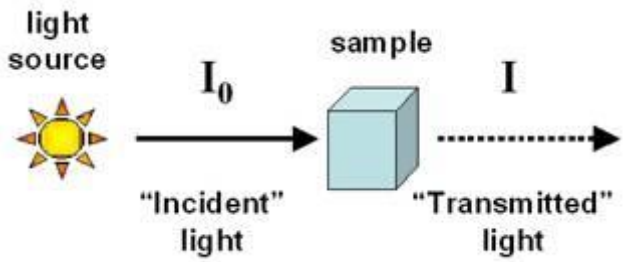

Figure 3.4.10 – *Transmittance [35].*

For the measure of the transmittance, the sample needs to be in place 2 and the two samples of $BaSO_4$ need to be placed in places 1 and 3 of **Figure 3.4.7**. Then is necessary to choose the *Transmittance* option in the software and click *Start* to begin the measurement. The result is a percentage of transmittance per wave length.

3.4.5.3. Absorbance

The light that is not reflected or transmitted is absorbed by the body, called absorbance. A schematic representation of this parameter is presented in **Figure 3.4.11**.

Figure 3.4.11 – *Reflectance, transmittance and absorbance*

As it has been mentioned this optical property has been calculated by the **equation 3.4.2** and not measured with the spectrophotometer.

3.4.6. Mechanical properties

This section of the chapter collects the different mechanical properties evaluated in this

Bachelor's project. As it has mentioned in the introduction part, one of the applications for this material is for make dental prostheses, so the Vickers hardness and the fatigue fracture are two important parameters to evaluate and characterize in order to know if the printed desired ceramic material accomplish the desired requirements.

3.4.6.1. Vickers hardness (HV)

Hardness is a measure of the resistance to localized plastic deformation [1]. In this regard, the Vickers hardness allows getting hardness parameters at different lengths scales. For this test a very small diamond indenter having pyramidal geometry, see **Figure 3.4.12a**, is forced into the surface of the sample, which creates a mark on the surface, see **Figure 3.4.12b**. The indenter, done of diamond, allows indenting hard and soft materials, in addition to allow getting measures from materials with small wall thickness, which is important for our samples, which are 2 or 3 mm thick.

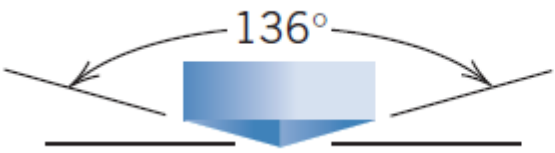

Figure 3.4.12a – *Vickers indenter [1].*

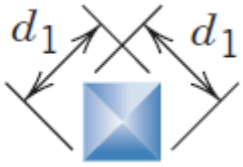

Figure 3.4.12b – *Indentation's mark [1].*

observed and the diagonals of the residual imprints measured by using the LSCM equipment. After that, Vickers hardness has been calculated by using the **equation 3.4.3**, where *P* refers to the applied load and *d* refers to mark's diagonal.

$$\mathrm{HV} = 1.854P/d_1^2 \qquad (3.4.3)$$

Akashi hardness tester (MVK-H0) has been used to determine the desired mechanical property, see **Figure 3.4.13**. The Vicker's hardness has been determined at 1 Kg of maximum applied load during 20 sec. This load has been chosen in order to get the mechanical response for the ceramic composite material. Per specimen it has been conducted four indentations per sample placed randomly, which allows getting a real measure by doing a mean of all the diagonals, always keeping in mind that if one indentation falls inside a pore the measure can't be considered.

Figure 3.4.13 – *Vickers hardness.tester.*

3.4.6.2. Fatigue cyclic indentation

Fatigue is a form of failure that occurs in structures subjected to dynamic and fluctuating stresses. Under these circumstances it is possible for failure to occur at a stress level considerably lower than the tensile or yield strength for a static load as in **section 3.4.6.1**. The term “fatigue” is used because this type of failure normally occurs after a lengthy period of repeated stress or strain cycling. This mechanical trial is important in our case because depends of the material’s final application, it will be constantly in stress periods [1].

In order to guarantee the good results it has simulated a fatigue fracture trial such as the material would be for a dental prosthesis aimed to adults or kids with tooth diseases or elderly people. In this Bachelor’s project, it has been chosen the more restrictive case, kids with tooth diseases. It has registered values of 425N as a masticatory force in kids with tooth diseases and values of 370N in adults with tooth diseases, whereas in elderly people the value is around 180N [36]. So the trial has done with a nominal value of 425N and a period of 1000 cycles. This trial has been done as a preliminary test and the number of cycles has been decided in order to see how the samples behaves under fatigue conditions. The different experiments have been conducted using an Instron® model 8511, see **Figure 3.4.14**.

Figure 3.4.14 – *Instron® 8511 fatigue machine.*

To do this test, the experiments have been conducted following a sinusoidal wave, as it is presented in **Figure 3.4.14**, where *N* is the nominal value (234 N), *C* is the crest (425 N, which means amplitude of 191 N), *Tr* is the trough (43 N) and finally the period is the inverse of frequency, *f*, it has worked with a frequency of 4 Hz which means a period of 0.25 sec per cycle.

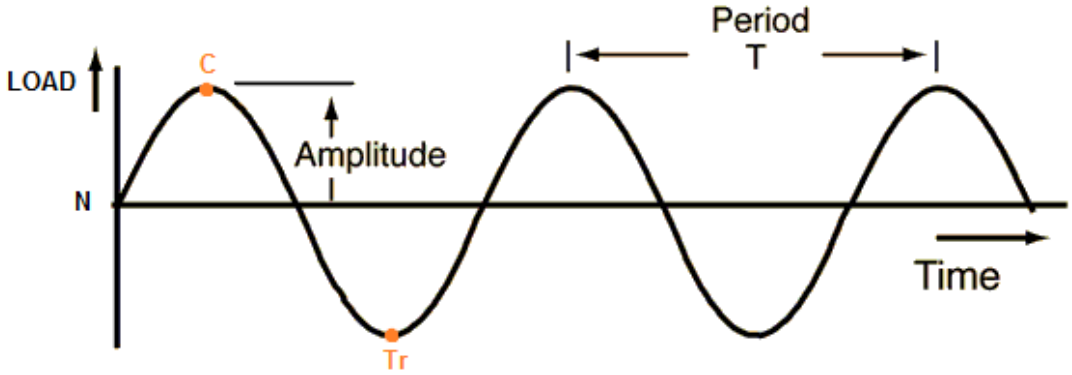

Figure 3.4.15 – *Sinusoidal wave representation for the cyclic tests conducted.*

These cyclic tests have been conducted under dry atmosphere as well as under water in order to simulate the body fluid (SBF).

The cyclic residual imprints have been observed by the *Anly* tool of the LSCM in order to observe the main deformation and fracture mechanisms activated under this particular conditions, see **Figure 3.4.16**. A reliable measurement of the residual imprint has been conducted by taking 4 diagonals of each residual imprint.

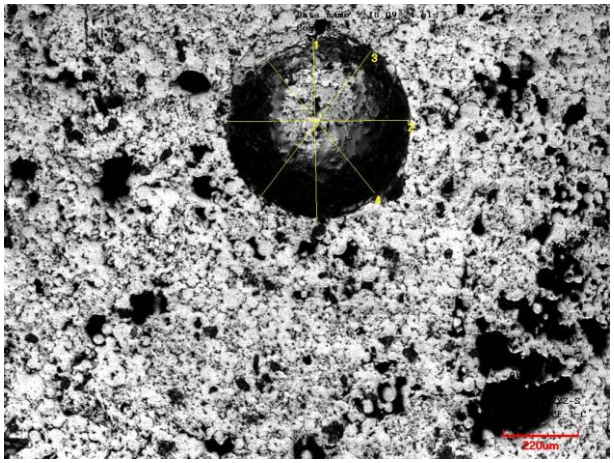

Figure 3.4.16 – *Residual imprint performed 95_1740 fatigue mark in dry atmosphere.*

4. Results and discussion

This main data obtained along this project are summarized and discussed along this section. Two main sections will be clearly presented; one corresponding to their microstructure and after that to their mechanical characterization.

Before all, it is necessary to clarify that the sample label 50_1450 with a 50 wt. % for each ceramic constituent (3Y-TZP and CeO_2)has not been possible of prepare due to the maximum temperature used in this Bachelor's project is not enough to sinter the material and reach densities around the theoretical.Only for this kind of specimens, some microstructural parameters has been determined; density and roughness analysis by means of the Archimedes' method and profilometry, respectively.

4.1. Microstructure

In order to get a general view of the printed ceramic materials previously the polishing process; four different images have been taken by means of LSCM as it is clearly presented in **Table 4.1.1**.

Table 4.1.1 – *Microstructure pictures.*

	Sintering temperature (ºC)	
	1450ºC	**1740ºC**
95% 3Y-TZP 5% CeO_2	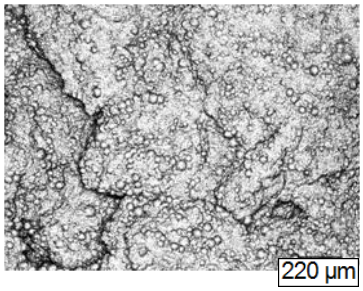	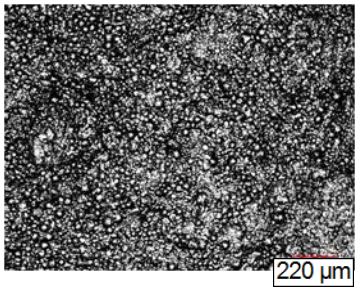
90% 3Y-TZP 10% CeO_2	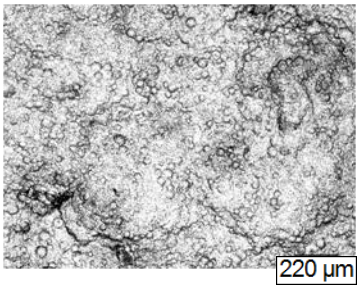	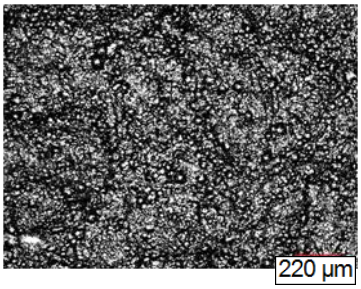
80% 3Y-TZP 20% CeO_2	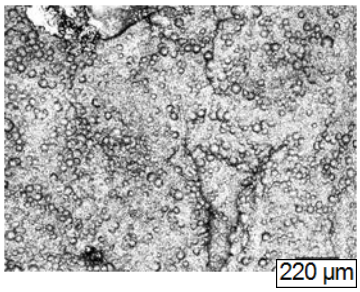	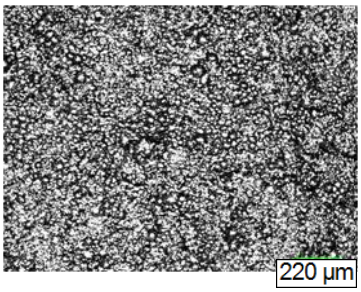
50% 3Y-TZP 50% CeO_2	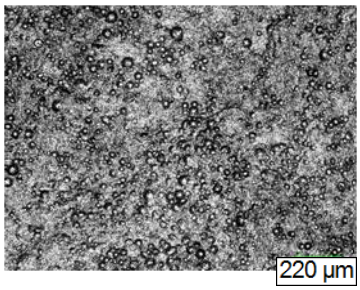	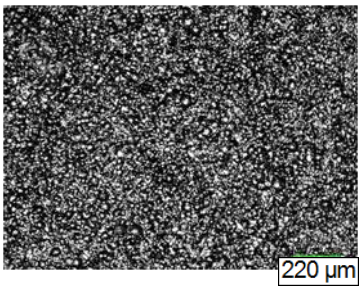

From the images observed and summarized in **Table 4.1.1.**, the surface topography observed by LSCM presents a rough specimen after the 3D-printing process and subsequent sintering process. The roughness is very high and the topography does not seem to be really suitable for accurate nanoindentation measurements. Furthermore, the porosity is not possible to clearly be distinguished from the images reported in this section and it is necessary to polish the specimens in order to reveal the porosity generated during the 3D-printing process as it will be presented in more detail in the on-coming section, see **section 4.1.1**.

4.1.1. Grain size

As it has been explained in **section 3.4.1** the samples 95_1450 and 95_1740 have been thermally treated to determine the grain size. FESEM micrographs for both sintering temperatures are presented in **Table 4.1.2**. In the upper part, a general view can clearly be observed while in the bottom part of this image, the grain size distribution can be appreciated. For both sintering temperatures, a bimodal grain size can clearly be appreciated. For the specimens sintered at 1450ºC, the resulting grain size is of around 470 nm; comparing this value to the conventional 3Y-TZP grain size which is around 300-350 nm, this different is the effect of the doping the zirconia material with ceria. On the other hand, for the samples sintered at 1740ºC, the specimen presents a grain size of 1000 nm. Here the ceria content does not play an important role compared to the temperature. It is known as reported in Ref. [37], that at sintering temperatures higher than 1500ºC, a phase transformation from tetragonal to cubic phase is activated producing a considerable increasing of the grain size.

Table 4.1.2 – *Grain size pictures by FIB.*

95_1450	95_1740
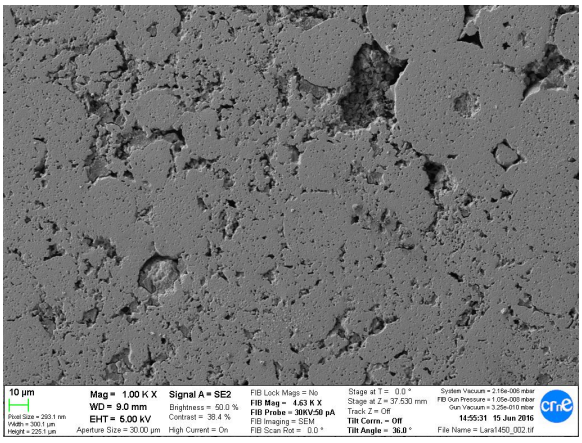	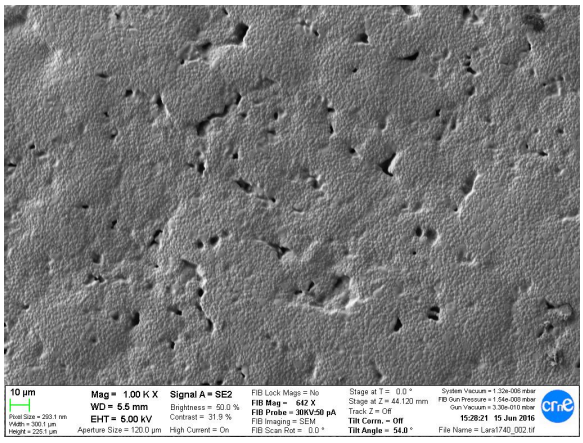
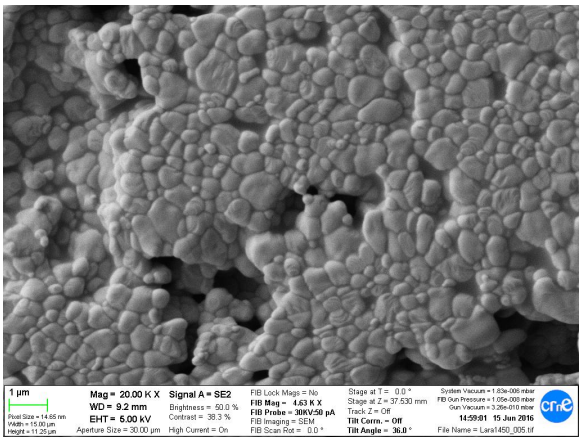	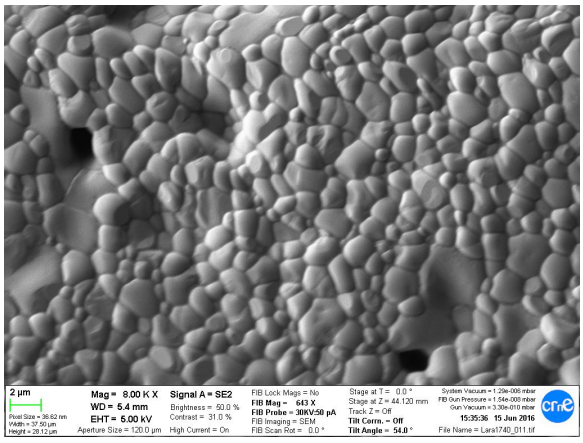

Table 4.1.3 summarizes the average grain size which has been determined by using the linear intercept method.

Table 4.1.3 – *Grain size values.*

	Sample	
	95_1450	95_1740
Grain size (μm)	0.474 ± 0.22	1.39 ± 0.44

4.1.2. Surface porosity

After polishing the specimens, two different images have been taken by means of LSCM equipment. One image per specimen is summarized in **Table 4.1.4**.

Table 4.1.4 – *Surface porosity pictures.*

	Sintering temperature (ºC)	
	1450ºC	**1740ºC**
95% 3Y-TZP 5% CeO_2	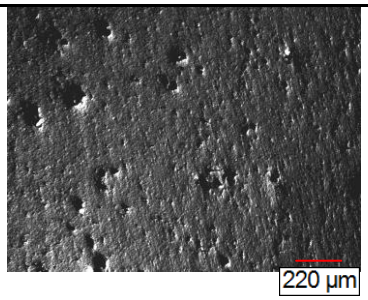	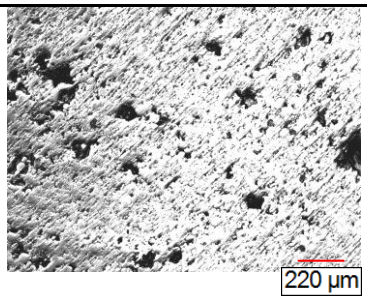
90% 3Y-TZP 10% CeO_2	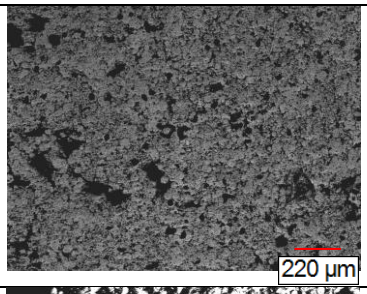	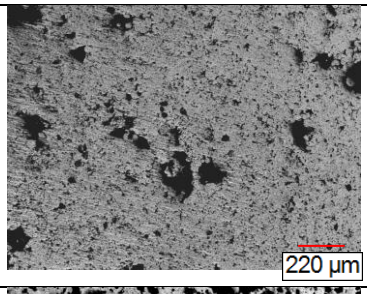
80% 3Y-TZP 20% CeO_2	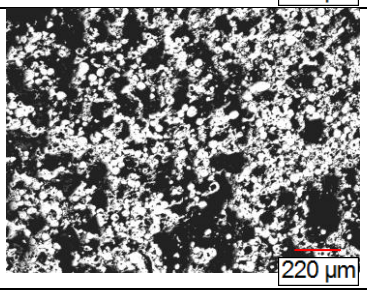	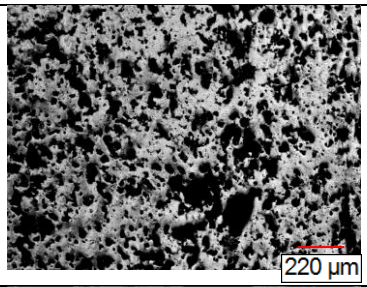
50% 3Y-TZP 50% CeO_2	----	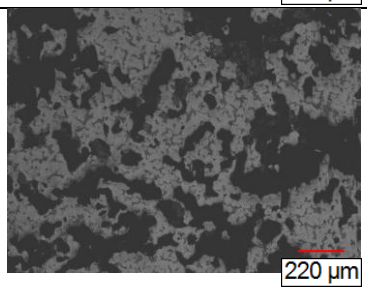

From the images summarized in **Table 4.1.4** is possible to see how the porosity decreases with the temperature increases. A similar trend is observed when the amount of CeO_2 decreases. Furthermore, form the above images the pore distribution presents a bimodal distribution (fine and coarse pore distribution). Mainly, this porosity is attributed to the gelling agent used to print these specimens.

In order to quantify the porosity by using the different LSCM images, the *Anly* tool from Imagej is used in order to determine the surface porosity. The arithmetic porosity for the seven

samples is summarized in **Table 4.1.5**.

Table 4.1.5 – *Surface porosity.*

Sample	Porosity (%)
95_1450	8.3 ± 0.3
95_1740	8.2 ± 0.5
90_1450	10.9 ± 0.8
90_1740	10.8 ± 2.2
80_1450	34.0 ± 5.0
80_1740	27.2 ± 4.9
50_1740	41.9 ± 2.6

The **Table 4.1.5** shows how the porosity decreases with the temperature and how the surface porosity increases when the ceria percentage is higher. These results are in agreement with the observation previously done by the LSCM images.

In order to get any trend, the different data presented in the previous table has been represented the porosity as an histogram as a function of the sintering temperature and ceria content for all the different samples investigated in this Bachelor's project, see **Figure 4.1.1**.

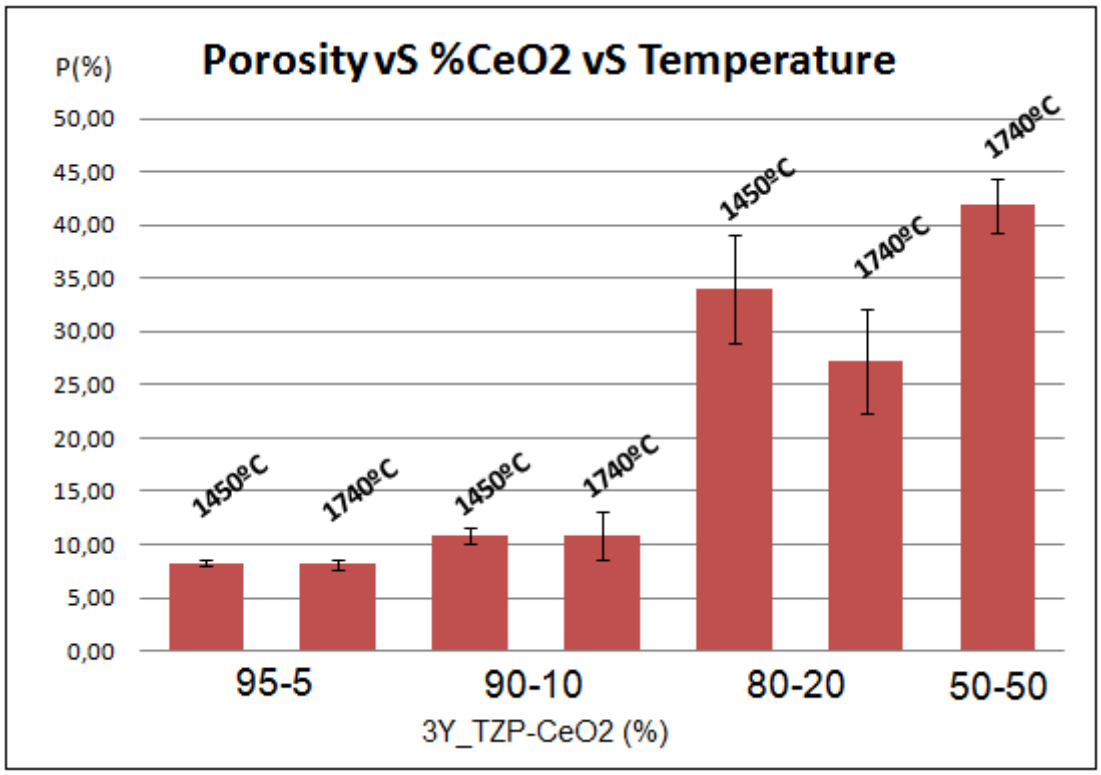

Figure 4.1.1 – *Surface porosity.*

As it is clearly presented in this image, the ceria content ranged between 5 to 10%, the sintering temperature does not affect to the porosity content plotted in the *y*-axis. However, when the ceria content is higher than 20 wt.%, the porosity increases considerably due to the maximum temperature employed does not allow to sinter the CeO_2 phase. For the specimen doped with 20 wt.% of ceria, the temperature decreases the surface porosity as it clearly is observed in **Figure 4.1.1**.

Finally, another microstructural parameter to characterize the porosity for the 3D-printed specimens is necessary to determine the pore size. To do that it has been taken four different measures per pore and it has been measured ten pores per sample. In this way, is possible to find a realistic estimation of this parameter as a function of the ceria content and temperature. **Table 4.1.6** shows the results, which have been obtained by means of the Image J software.

Table 4.1.6 – *Pore size.*

Sample	Pore size (µm)
95_1450	112.8 ± 58
95_1740	125.4 ± 66
90_1450	97.6 ± 38
90_1740	116.3 ± 62
80_1450	98.8 ± 39
80_1740	134.7 ± 31
50_1740	161.7 ± 66

The results of **Table 4.1.6** show how the pore size decreases with the temperature.

4.2. Density

This subsection shows the results of the obtained values from the Archimedes' method with the values obtained by using the rule of mixtures [1]:

$$\rho = \sum_{i=1}^{n} \rho i \cdot vfi \qquad (4.2.1)$$

Where ρ is the final density, ρi is the theoretical density of each material and vfi is the volume fraction of each material.

Table 4.2.1 summarizes the density determined by the Archimedes method and the theoretical density determined by using **equation 4.2.1**.

Table 4.2.1 – *Density values determined by the Archimedes method and theoretical density determined by the rule of mixtures.*

Sample	Experimental density (g/cm^3)	Theoretical density (g/cm^3)
95_1450	4.8 ± 0.4	6.1
95_1740	5.4 ± 0.3	
90_1450	5.0 ± 0.6	6.2
90_1740	5.4 ± 0.3	
80_1450	5.5 ± 0.6	6.4
80_1740	5.3 ± 0.5	
50_1450	5.2 ± 0.4	6.9
50_1740	5.7 ± 0.2	

Table 4.2.1 is possible to see how the density increases with the temperature for each particular condition. On the other hand density does not really follow the same rule with the CeO_2 content, it should increase theoretically, but this principle is not always fulfilled in reality. The density is directly affected by several effects; gelling agent as well as the printing density. All the samples have been printed with the same printing density, but these differences in the experimental density probably may be related to several heterogeneities produced during the sample preparation (i.e. precipitation of one of the ceramic specimens, etc.).

As it is shown in **Figure 4.2.1**, for the sintered samples at 1450ºC, the experimental density increases with the CeO_2 percentage except for the sample 50_1450, which is not representative due to the sintering temperature is not enough to densify the CeO_2.

Furthermore, it is necessary to mention that all the samples present an experimental density lower than theoretical. This difference may be attributed that by using the rule of mixtures, the density employed for the 3Y-TZP as well as for the CeO2 specimens corresponds to the dense specimens, with a pore density less than 1% In this regard, the printed material cannot present the same compactness due to the printing process because of the printed fibers present spaces between the different layers. Due to these, the experimentally and theoretical density does not fit.

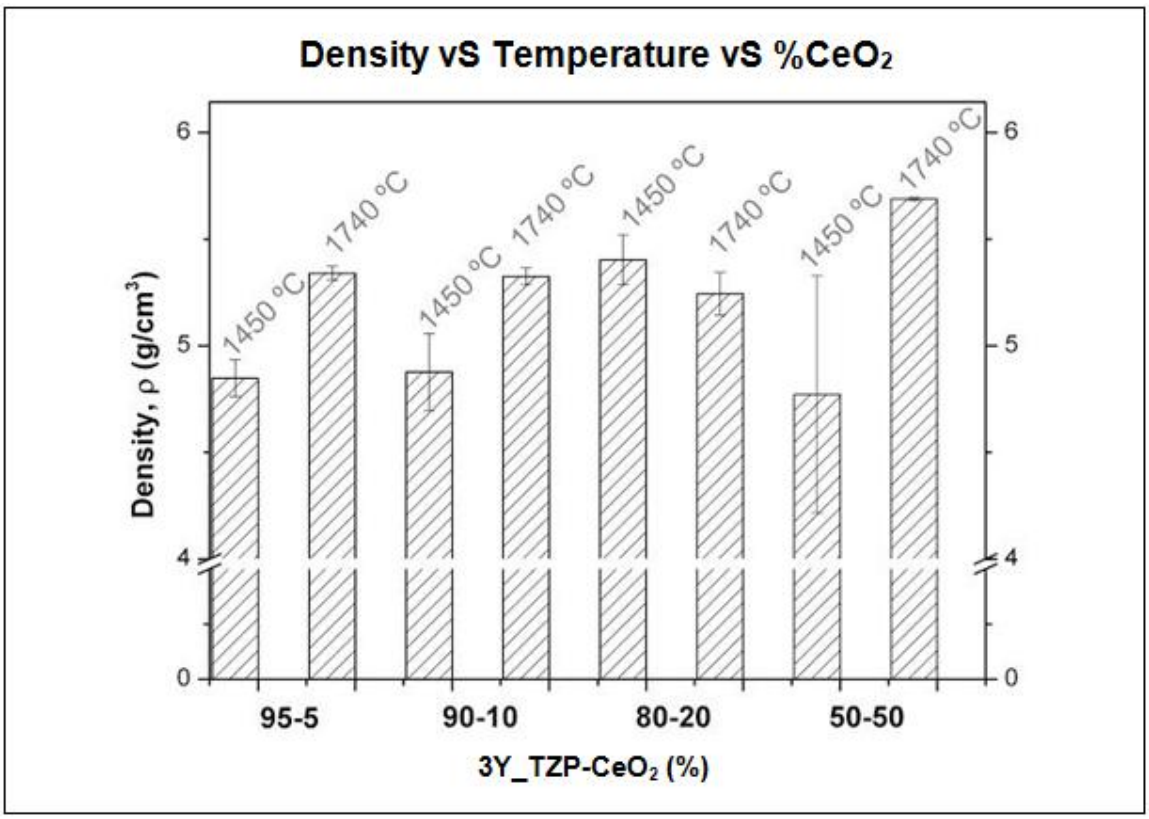

Figure 4.2.1 – *Density vs Temperature for each specimen.*

4.3. Roughness

As it has been mentioned in **section 3.4.3.1** a profilometer has been used to determine the main roughness parameters by doing *Map Scans* of the printed surfaces. By this analysis, it is possible to get R_a, R_q, R_z and R_t parameters, see **Table 4.3.1**

Table 4.3.1 – *Roughness parameters*

Sample	R_a (µm)	R_q (µm)	R_z (µm)	R_t (µm)
95_1450	68	81	531	398
95_1740	65	78	428	387
90_1450	93	107	453	442
90_1740	47	59	372	372
80_1450	39	53	399	399
80_1740	61	80	451	468
50_1450	62	70	414	408
50_1740	30	37	215	236

The data summarized in **Table 4.3.1** are presented in **Figure 4.3.1** in order to clearly appreciate the temperature as well as the CeO_2 content with the roughness parameters.

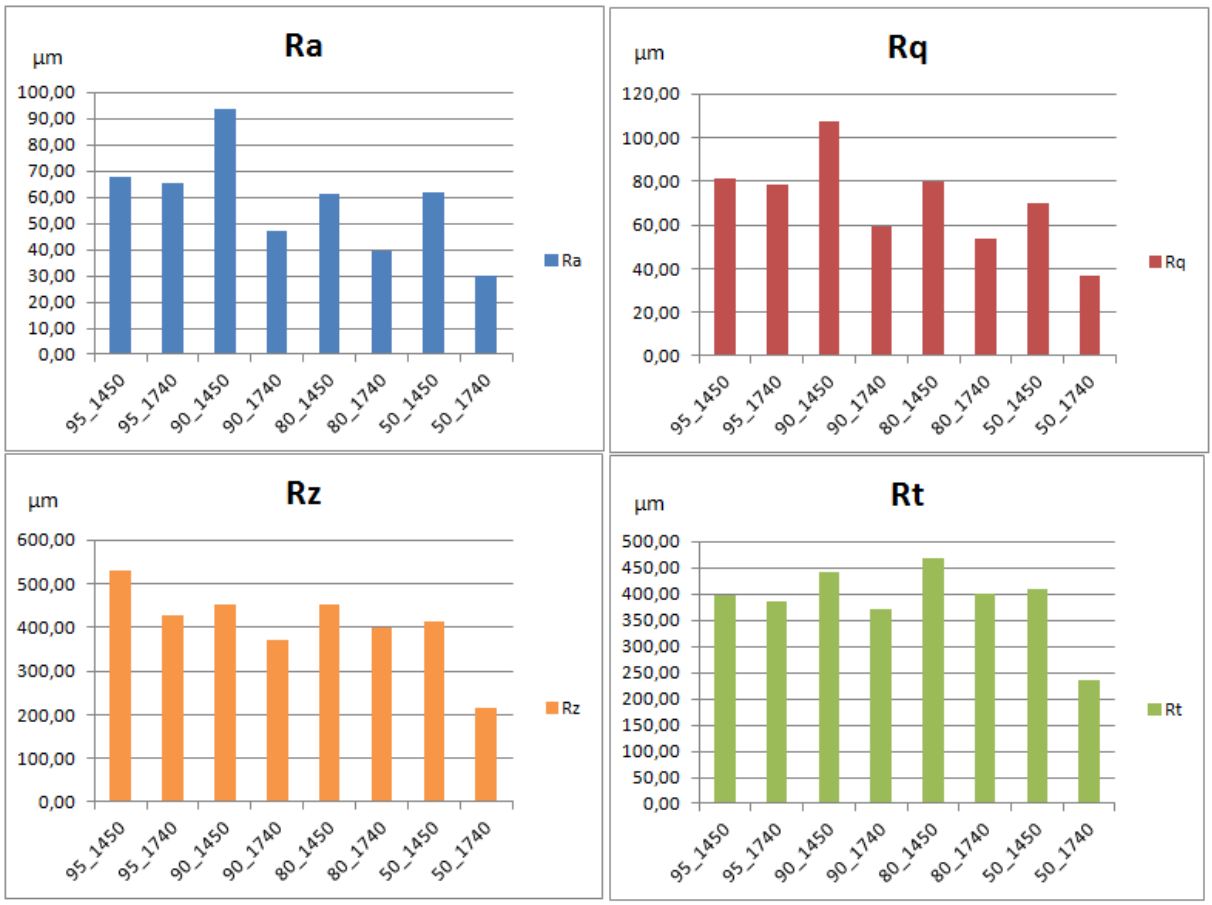

Figure 4.3.1 – *R_a, R_q, R_z and R_t graphics*

As it is depicted in **Figure 4.3.1**, is possible to observe that all roughness parameters presented above are affected by the sintering temperature. It is predictably because as we previously observed and presented in **Figure 4.1.1**, the specimens sintered at low temperature (around 1450 ºC), presents higher pore density. Another interesting point to highlight is that the sample 50_1740, all roughness parameters are smaller than for the other specimens. This may be attributed due the polishing process for this specimen is easy than for the others due to the high amount of cerium content.

It is possible to affirm that for the samples sintered at 1740ºC, which are the ones that are well sintered if we focus on the ceria content, the R_a and R_q decreases with the ceria content. Both parameters are the main parameters to characterize the roughness. On the contrary, the samples sintered at 1450ºC do not present any trend; this may be related to the huge present of heterogeneities that this specimens have, mainly porosity.

4.4. Optical properties

In this section the optical properties for the specimens investigated here are summarized. As it has been previously explained in **section 3.4.5**, it has been used a spectrophotometer to get values of reflectance (*R*), transmittance (*T*) and absorbance (*A*). The results are summarized in the Appendix A.

The transmittance (*T*) has been obtained just for the samples with 5 wt.% of CeO_2 sintered at 1450 and 1740ºC in order to see how the optical properties are affected by the temperature, see **Figure 4.4.1a**. As it can observe, the transmittance for the sample sintered at 1450ºC ranges between 0 to 2.5%. On the other hand, the sample sintered at 1740 ºC, this value ranges between -1 to 1.5%. Both temperatures presents an artifact, where the transmittance measure is not representative from the measurements for a wavelength of around 2000 nm, . From these results it is possible to omit the transmittance because a percentage ranged between 1 or 3 % is not significant due to this value is in the range of the equipment detection. So, for the rest of the samples, it has been obtained just the reflectance and calculated the absorbance.

What we can observe in the other tables (see Appendix A) and in the **Figure 4.4.1b** is that the reflectance is directly proportional to the wavelength and, due to **equation 3.4.2** and omitting transmittance, the absorbance is inversely proportional to the wavelength.

Generally, as **Figure 4.4.1a** shows, the reflectance increases with the temperature but decreases with the ceria percentage. For that reason, in visible spectrum, colored in blue in **Table A.1**, the reflectance is around 45% value for the samples with a 5 wt.% Cerium content with two different sintering temperatures. As we mention in the introduction part, these materials were developed for dentistry applications. In this sense, dentistry looks for a material that does not totally reflects the light, for this reason ceria is a good option to combine with zirconia to obtain a prostheses, ceria provides with its yellow color, similar to the real teeth, and with reducing the reflectance.

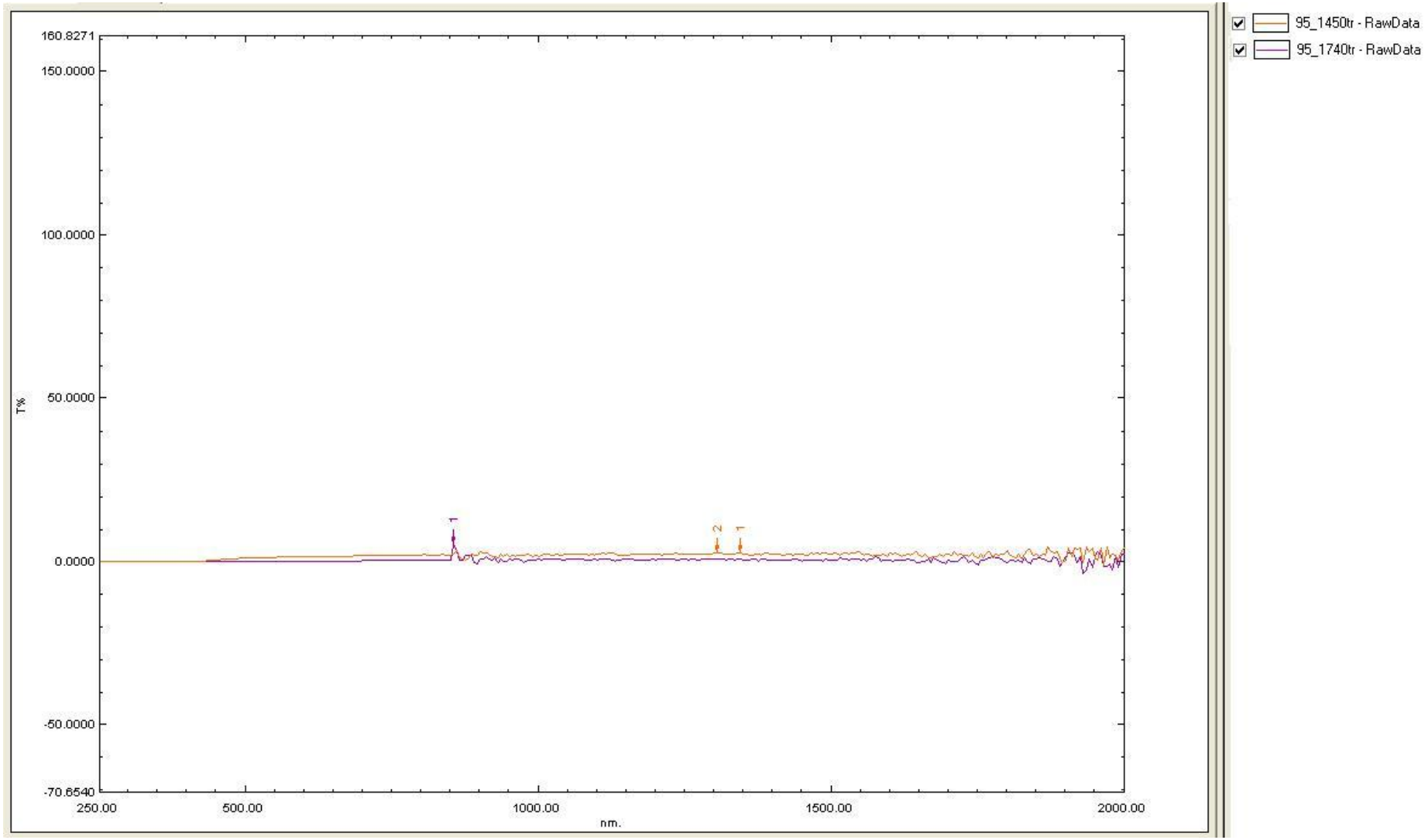

Figure 4.4.1a –*Transmittance vS Wavelength graphic.*

ETSEIB

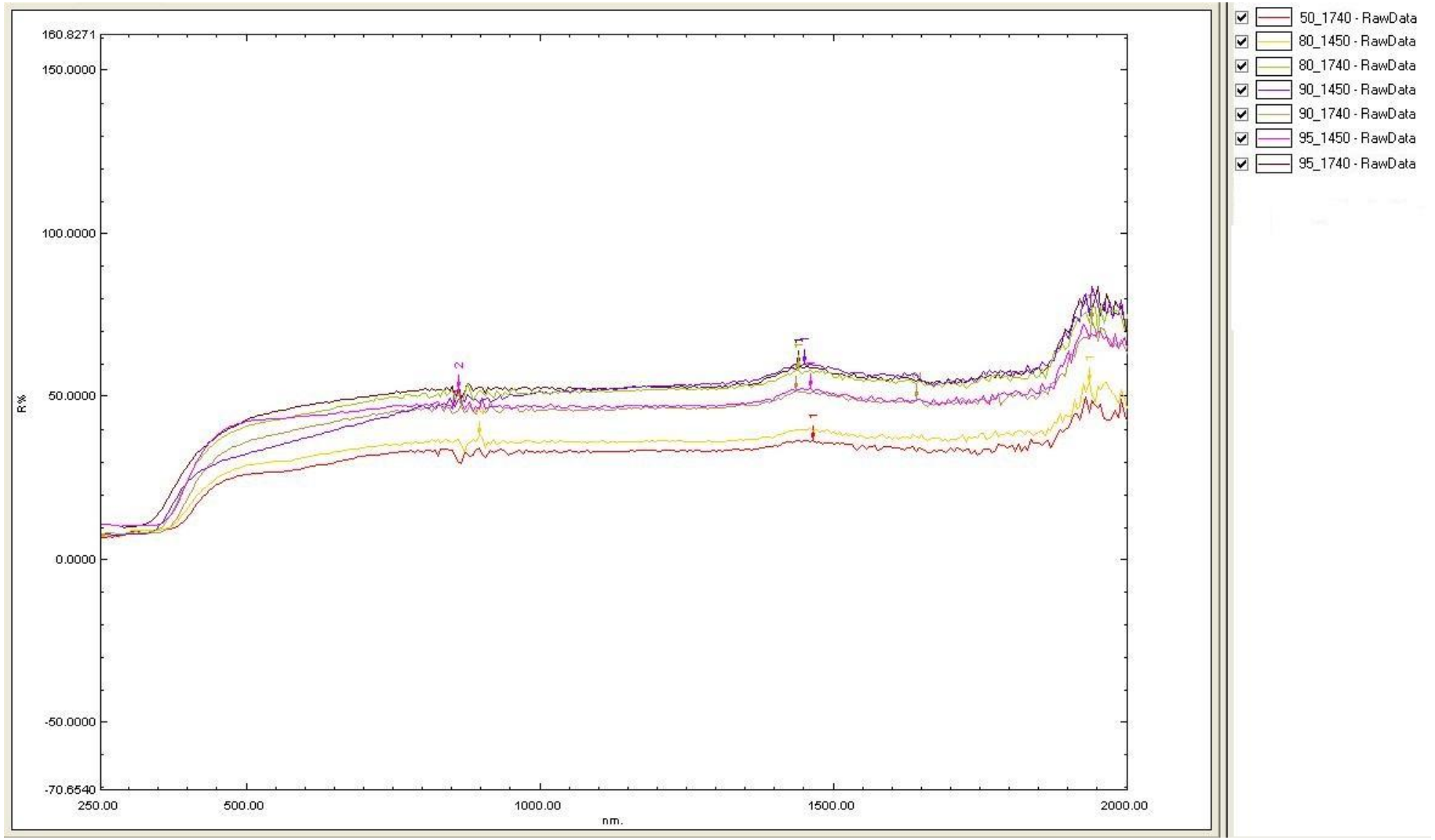

Figure 4.4.1b – *Reflectance vS Wavelength graphic.*

4.5. Mechanical properties

4.5.1. Vickers hardness

In order to determine the Vickers hardness (HV), the two diagonals of the mark may be measured to calculate the arithmetic mean diagonal, see **Figure 4.5.1**. This arithmetic mean, *d* summarized in **Table B1** (Appendix B) allows to directly determine Vickers hardness.

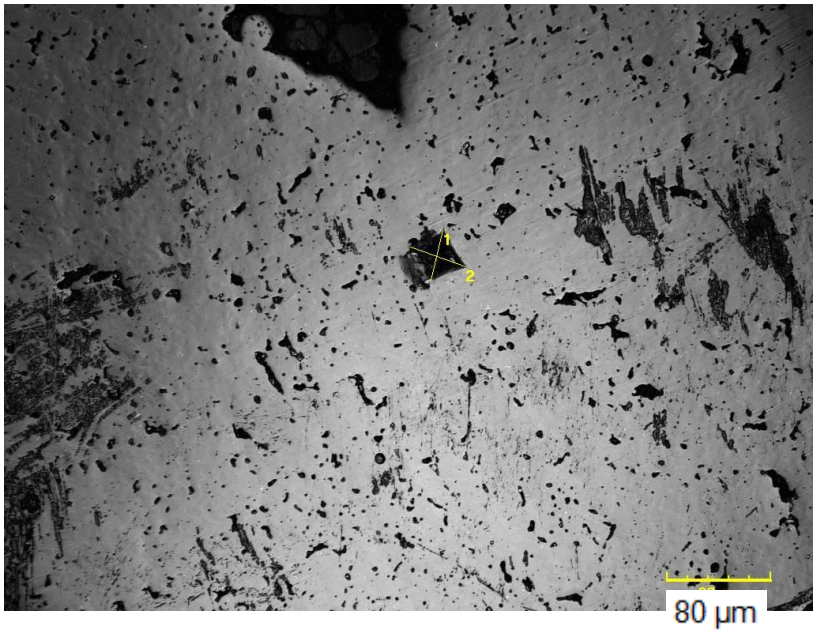

Figure 4.5.1 – *Indentation in sample 95_1450.*

The Vickers hardness determined for all the specimens at 1 kgf are presented in **Figure 4.5.2**. In this representation is possible to see that the Vickers hardness does not follow a trend. However, it is possible to observe a slightly Vickers hardness reduction when the ceria content increases. The specimen with a higher Vickers hardness is the specimen with a ceria content of 5% and sintered at 1450ºC. On the other hand, one aspect an increasing of the Vickers hardness when the sintering temperature increases due to at this temperature a phase transformation from tetragonal to cubic phase may occur. However, this change has not clearly been observed due to the high porosity content.

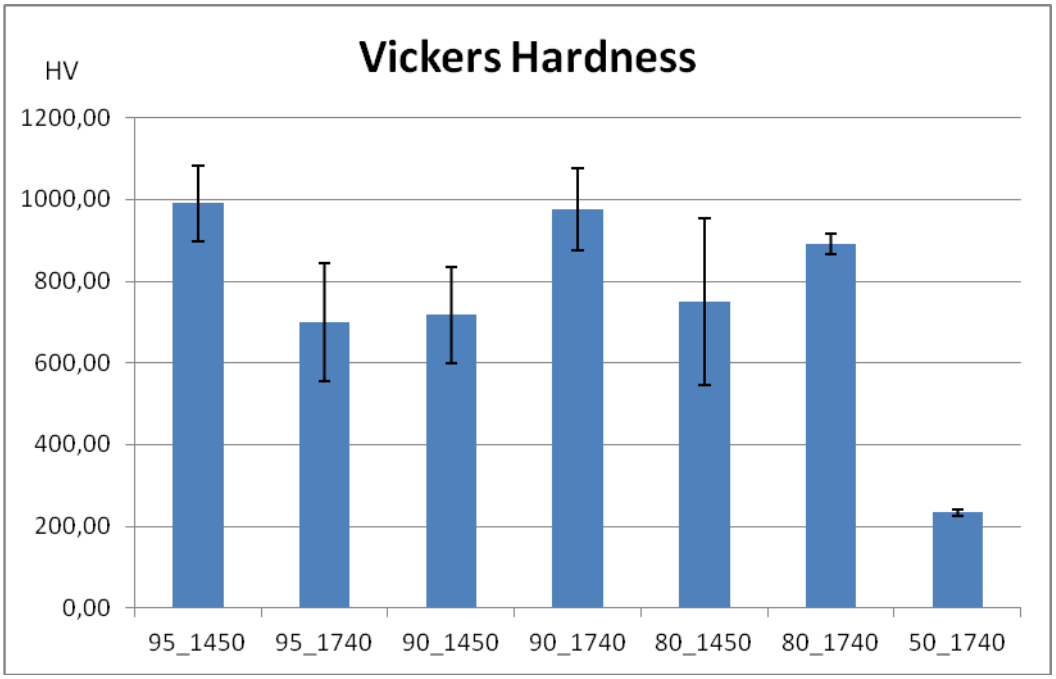

Figure 4.5.2 – *Vickers hardness per sample graphic.*

Figure 4.5.3 represents the Vickers hardness as a function of the porosity for all the specimens investigated here. In this graphic is possible to observe that the Vickers hardness decreases with the porosity. However, for two different samples (95_1740 and 90_1450) does not exhibit this trend. One would expect that the hardness for the specimens sintered at 1740ºC will be higher than those sintered at 1450ºC, due to at temperatures higher than 1500ºC a cubic phase can be induced as reported Roa and co-workers in Ref. [37] due to the cubic phase is harder than the tetragonal phase. However, this abnormal behavior in terms of Vickers hardness may be related to the porosity heterogeneously distributed in the studied specimens.

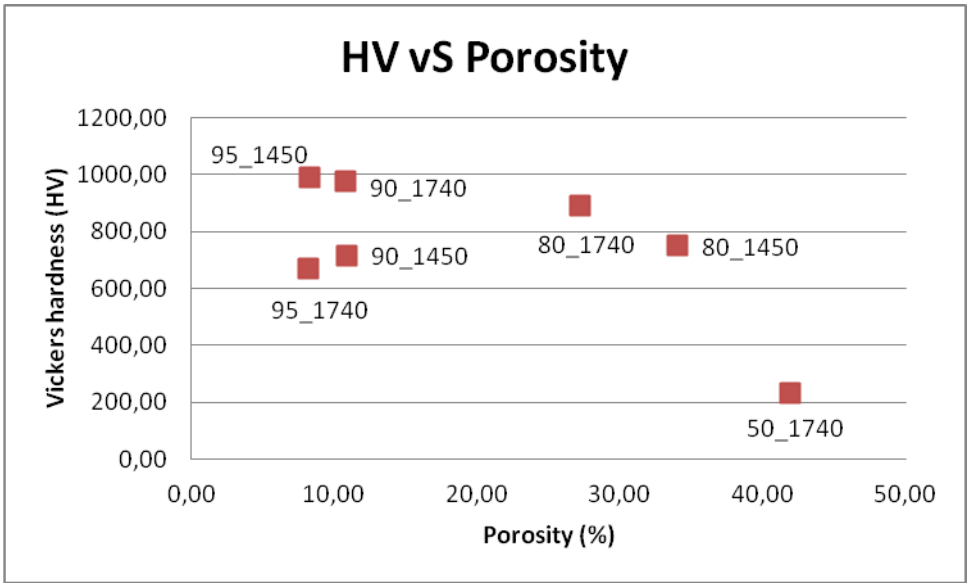

Figure 4.5.3 – *Vickers hardness-Porosity graphic.*

4.5.2. Hertzian contact fatigue

In order to use these composite materials as dental prostheses one of the most important factors is the contact fatigue fracture, because teeth are in constant fatigue, so it is necessary to ensure that our material would survive to the mastication cycles.

As it has been explained in the experimental part (**section 3.4.6.2**), a load of 425N was used to investigate this behavior under two different conditions. **Table 4.5.1** summarizes the fracture damage for each investigated specimen.

Table 4.5.1 – *Fatigue fracture results.*

Sample	Atmosphere	Result	Comments
95_1450	Dry	**OK**	The sample survives without problems.
	Water	**OK/KO**	The sample breaks with 20N of pre-load but not by the application of the load point.
95_1740	Dry	**OK**	The sample survives without problems.
	Water	**OK**	The sample survives without problems.
90_1450	Dry	**KO**	The sample breaks at 300 cycles (see **inset**). 
90_1740	Dry	**OK**	The sample survives without problems.
	Water	**OK**	The sample survives without problems.
80_1450	Dry	**KO**	The sample breaks before the trial, when it is tightened to the support. 
80_1740	Dry	**KO**	The sample survives to the 1000 cycles but breaks at the end. 
50_1740	Dry	**KO**	The sample breaks at the first contact without any cycle. 

The sample with 5 wt.% content and sintered at 1450 ºC survives after 1000 cycles as it is summarized in **Table 4.5.1**. On the other hand, the same specimen under water does not survey. This observation highlights that the different specimens behaves different for the same sintering temperature under different atmospheres due to their heterogeneities (porosity distribution, etc.) As we mention in the previous **Table**, the sample has not broken for the

application load point; it has broken probably for the tightened process to subject the sample.

A similar trend has been observed for the specimen sintered at 1740ºC with a 10 wt.% content of ceria as for the specimen tests under water with a 5 wt. % content. In this case, one corner breaks at the end of the cyclic test. So the sample reaches 1000 cycles, and the reason of this failure is attributed to the subjecting process and not to the cyclic test.

The specimens with 5 and 10 wt. % ceria content sintered at 1740 ºC do not break under dry atmosphere. However, the other specimens investigated in this Bachelor's project breaks catastrophically under these conditions.

Figures 4.5.4 and **4.5.5** exhibits the residual imprints performed under LSCM for the specimens tested under dry atmosphere.

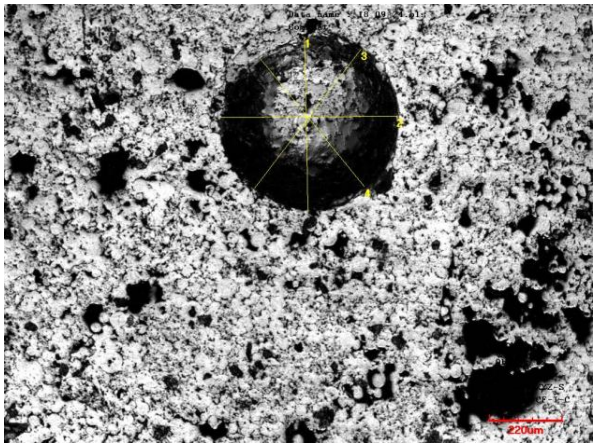

Figure 4.5.4a – *95_1740 fatigue mark in dry atmosphere.*

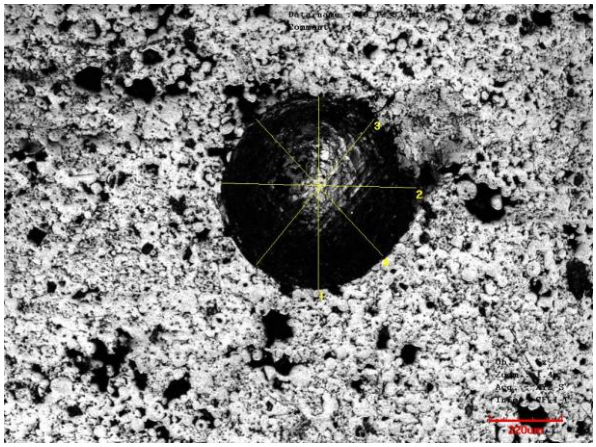

Figure 4.5.4b – *95_1740 fatigue mark in water atmosphere.*

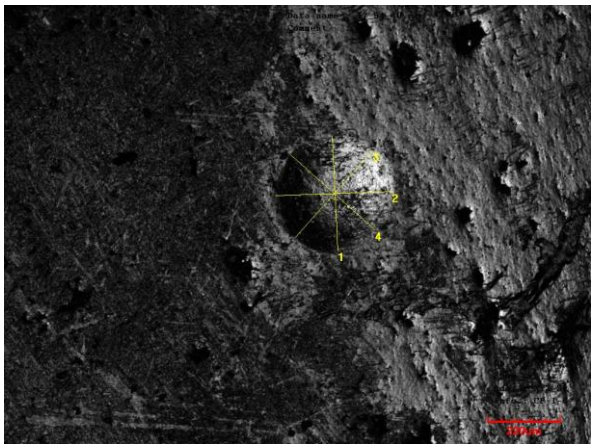

Figure 4.5.5a – *90_1740 fatigue mark in dry atmosphere.*

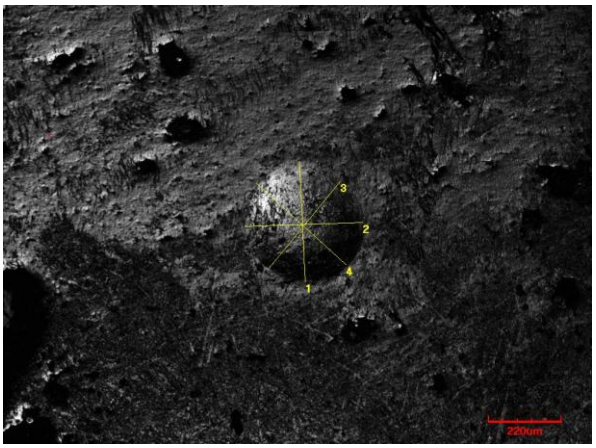

Figure 4.5.5b – *90_1740 fatigue mark in dry atmosphere.*

ETSEIB

All the residual imprints presented in **Figure 4.5.5** have been taken at the same magnification for comparison purposes.

For the specimen with a cerium content of around 5 wt.% and sintered at 1740ºC; the residual spherical imprint is bigger under SBF than under dry conditions (592 and 536 µm, respectively). Similar result has been observed for the specimen doped with 10 wt.% and sintered at 1740 ºC. In this particular case the mark in dry atmosphere (358.92 µm) is smaller than under SBF (359 and 368 µm, respectively). For all the residual imprints observed by LSCM, no crack or damage has been clearly been observed by LSCM.

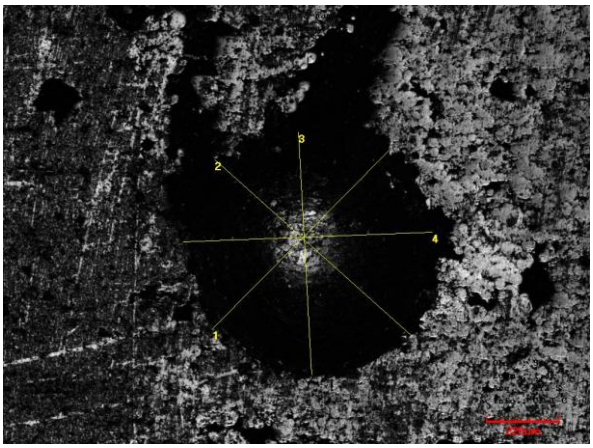

Figure 4.5.6a – *95_1450 fatigue mark in dry atmosphere.*

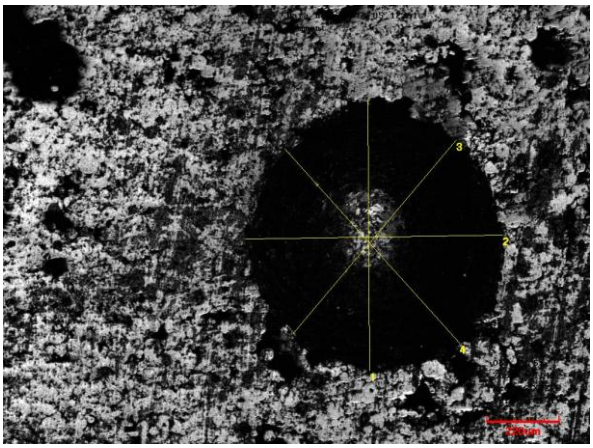

Figure 4.5.6b – *95_1450 fatigue mark in water atmosphere.*

In this case, both marks are the biggest ones for the two tests. The sample 95_1450 tested in dry atmosphere has a mark of 784.98 µm, and the sample 95_1450 tested in water atmosphere has the biggest mark with a diameter of 815.60 µm. It is necessary to remember that this sample contains a 5% of not sintered ceria, which means less hardness and less fatigue resistance, in the end, a shorter life cycle.

Conclusions

From an analysis of the experimental results obtained in this Bachelor's project, the following conclusions can be drawn:

- Microstructural and mechanical properties are strongly affected by the ceria content as well as by the sintering temperature.
- Sintering temperature produce a strong effect on the microstructural parameters, yielding a high density as well as less pore density for the specimens sintered at 1740ºC.
- Transmittance is not affected by the temperature as well as for the cerium content, while the absorbance is strongly dependent.

    - CeO_2 content used to make the samples affects directly to the mechanical properties, which are poor when the quantity of ceria is greater than a 10%.

    - Mechanical properties in terms of Vickers hardness and Contact fatigue are higher when the ceria content is around 5 wt. % and sintered at 1740ºC.

Nowadays we are far away from print dental prostheses from home with a polymer 3D-printer adjusted to ceramics printing, but the results of this study makes us to believe that ,with more researches and better adjustments to the machines, the dental technicians will change their fabricating processes and 3D-printing techniques will be their main tool.

Economic impact

The budget for this Bachelor's work has been done considering different factors: specialized staff, material, products, energy and trials. In the following table the costs are summarized.

MATERIAL COST			
Product	**Quantity**	**Cost per unit**	**Cost**
3Y-TZP	500 g	150 €/Kg	75.00 €
CeO_2	60 g	183.5 €/Kg	11.00 €
Agar-Agar	20 g	100 €/Kg	2.00 €
Water	15 m^3	0.62 €/m3	9.30 €
Saint Govain 30µm polish suspension	0.3 L	110 €/Kg	33.00 €
Saint Govain 6µm polish suspension	0.25 L	90 €/Kg	22.50 €
Saint Govain 3µm polish suspension	0.25 L	90 €/Kg	22.50 €
Buehler Mastermet 2 colloidal Silica 1µm suspension	0.1 L	180 €/Kg	18.00 €
Struers MD-Piano 320 polishing disc	1 u.	100 €/u.	100.00 €
Struers MD-Piano 600/1200 polishing disc	2 u.	100 €/u.	200.00 €
Struers MD-Plan	1 u.	65 €/u.	65.00 €
Struers MD-Dac	2 u.	65 €/u.	130.00 €
Struers MD-Nap	1 u.	90 €/u.	90.00 €
Bakelite	650 g	8 €/Kg	5.20 €
Laboratory paper	2 u.	0.5 €/u.	1.00 €
SUBTOTAL 1			784.50 €

EQUIPMENTS USE COST			
Trial	**Quantity**	**Cost per unit**	**Cost**
3D-printer	40 h	15 €/h	600.00 €
Heating magnetic stirrer	7 h	5 €/h	35.00 €
Sonicator	1.5 h	5 €/h	7.50 €
Nabartherm furnace	160 h	15 €/h	2,400.00 €
Archimedes test	1.5 h	5 €/h	7.50 €
Profiler	8 h	40 €/h	320.00 €
Mounting machine	2 h	5 €/h	10.00 €
Polishing machine	40 h	15 €/h	600.00 €
Confocal laser microscope	35 h	50 €/h	1,750.00 €
Vickers micro testing machine	3 h	15 €/h	45.00 €
Spectrophotometer	5 h	40 €/h	200.00 €
Fatigue machine	5 h	40 €/h	200.00 €
FIB	5 h	40 €/h	200.00 €
SUBTOTAL 2			6,375.00 €

OTHER COSTS	
Concept	**Cost**
Laboratory's material	170.00 €
Laboratory use	1,400.00 €
Office's material	35.00 €
SUBTOTAL 3	1,605.00 €

PROJECTIST'S ENGINEERING COST			
Concept	**Quantity**	**Cost per unit**	**Cost**
Sample preparation	100 h	10 €/h	1,000.00 €
Samples characterization	75 h	10 €/h	750.00 €
Results analysis	50 h	10 €/h	500.00 €
Memory development	125 h	10 €/h	1,250.00 €
SUBTOTAL 4			3,500.00 €

SUPPORT ENGINEERING COST			
Concept	**Quantity**	**Cost per unit**	**Cost**
Bachelor's degree tutor	50 h	40 €/h	2.000,00 €
Laboratory technician	9 h	40 €/h	360,00 €
SUBTOTAL 5			2.360,00 €

FINAL PROJECT'S COST	
Concept	**Cost**
Material cost	784.50 €
Equipments use cost	6,375.00 €
Other costs	1,605.00 €
Projectist's engineering cost	3,500.00 €
Support engineering cost	2,360.00 €
TOTAL	14,624.50 €

Environmental impact

The **main environmental impact** is the chemical wastes produced from samples preparation (**electricity** from the 3D-printer as well as the furnace used to sinter the specimens) as well as the **polishing wastes** coming from the diamond slurries.

The materials studied during this Bahcelor's degree aren't dangerous or contaminating, but most of their rests have been putted on specific trash cans in order to be recycled or treated, the rest has gone throw the waste pipe during the cleaning material processes.

Regarding to polish process, the polishing discs have been placed in the fitted up containers in order to be treated. The diamond slurries have gone throw the waste pipe with the water used during the polish process, but these waste pipes contain different filters, which catch the most of the diamond slurries rests, due to the sizes of its particles not all the solution can be filtered.

But the main environmental impact has been the electricity, all the machines used for sample preparation and for sample characterization use electricity, and some of them have been working during long periods as *Nabartherm* furnace, which has been working during periods ranged between 20 to 25 h. This electrical energy has been supplied for an electrical company which uses a little percentage of removable energies in order to obtain it, so it can reduce the environmental impact.

Future work

In reference to improve the 3D-printing process it would be convenient:

- Modify the syringe size; make it bigger to allow the possibility of print bigger figures or with more layers. The possibilities for print different figures are very limited due to that the quantity that fits in the syringe is very lacking.

- Design a pressurized extruding process to get a continue extruding process during all the print time, the discontinuities affect directly to the microstructure and to the mechanical properties of the printed figures.

- Reformulate the paste in order to improve the extrusion continuity in the printing process. The paste needs to be more viscous and fluent; the paste that we have gotten is as a gelatin in little pieces.

It must not be forgotten that we have been working with a gelling agent in order to make the ceramic paste printable.

In reference to continue with the study of the samples it would be convenient:

- Repeat all the process with the samples sintered at 1740ºC with a doping content ranged between 5 to 10 wt.% (95_1740 and 90_1740) using 12Ce-TZP instead of CeO_2, which has not been used because the difficulty to obtain it:

    - Analyze the microstructure by using X-ray diffraction to verify the different crystallographic phases (tetragonal, monoclinic and cubic).

    - Try to adjust the sintering temperature to get the best mechanical properties; as a function of the sintering temperature for the specimens doped with 5 and 10 wt. % of CeO_2.

    - Perform cyclic experiments for 1.000.000 cycles in order to simulate 3 years of continue mastication process at different mastication loads.

Acknowledgements

Firstly, I would like to thank to Emilio Jiménez, who introduced me to the amazing ceramic's world.

Thanks to the entire CIEFMA group, for let me develop my Bachelor's project in their facilities and use their machines.

I would give a special acknowledgement to my labmates Ferran Crespo, Albert Moreno and Dani López, who helped me to bear all the laboratory hours.

But most of all, I would like to express my sincere acknowledgement to Joan Josep Roa, who has not let me down during the development of this project and who has been my support these months.

Bibliography

[1] WILLIAM D. C., Jr. *Materials Science and Engineering* John Wiley & Sons, Inc 2007, 7th Edition.0. pp 5-13. ISBN: 978-0-471-73696-7

[2] PICONI C.; MACCAURO G. *Zircona as a ceramic biomaterial*. Biomaterials 20, 1999; pp 1-25.

[3] KANCHANA, S.; HUSSAIN, S. *Zirconia a Bio-inert Implant Material*. IOSR Journal of Dental and Medical Sciences Sciences V12 I6, 2013; pp. 66-69.

[4] BASU, B.; VLEUGELS, J.; VAN DER BIEST, O. *Toughness tailoring of yttria-doped zirconia ceramics.* International Material Review, 50, 2005; pp 239-256.

[5] MATERIALS DESIGN, INC. *Temperature-Dependent Phase Transitions of ZrO_2*. Materials Design Magazine. USA, 2000: pp 1.

[6] MADFA, A.; AL-SANABANI, F.; AL-QUDAMI, N.; AL-SANABANI, J.; AMRAN, A. *Use of Zirconia in Dentistry: An Overview.* The Open Biomaterials Journal, 5, 2014; p 1-3.

[7] CHEVALIER, J. *What a future for zirconia as a biomaterial?* Biomaterials 27, 2005; pp 536-537.

[8] CALES, B.; STEFANI Y. *Mechanical properties and surface analysis of retrieved zirconia femoral hip joint heads after an implantation time of two to three years.* 1999; pp 376-380.

[9] McLEAN, JW. *Evolution of dental ceramics in the twentieth century.* J Prosthet Dent Vol.85 2001; pp 61-66.

[10] RAMESH, T.R.; GANGAIAH M.; HARISH P.V.; KRISHNAKUMAR U.; NANDAKISHORE B. *Zirconia Ceramics as a Dental Biomaterial*. Bangalore vol. 85, 2012; p 154-160.

[11] BECHER, P.F.; SWAIN, M.V. *Grain-size dependent transformation behaviour in polycrystalline tetragonal zirconia.* Journal of the American Ceramic Society, 75, 1992: pp 493-502.

[12] HANNINK, R.H.J.; KELLY, P.M.; MUDDLE, B.C. *Transformation toughening in zirconia-containing ceramics.* Journal of the American Ceramic Society, 83, 2000: pp 461-487.

[13] BIRKBY, I. *Fabrication and Wear of Yttria Tetragonal Polycrystals*. University of Leeds PH.D. Thesis, 1994: pp 124-126.

[14] MATZKE, H. *Diffusion in Nonstoichiometric Oxides.* Academic Press Inc., London, 1981 pp 155-232. ISBN: 0-306-44051-2

[15] MOGENSEN, M.; SAMMES N.; TOMPSETT, G. *Physical, chemical and electrochemical properties of pure and doped ceria.* Solid State Ionics, 129, 2000; pp 63-94.

[16] ZACHAU-CHRISTIANSEN, B.; JACOBSEN, T.; SKAARUP, S. *Electrochemical determination of oxygen stiochiometry and entropy in oxides*. Solid State Ionics, 86-8, 1996; pp 725-731.

[17] VAREZ, A.; GARCIA-GONZALEZ, E.; SANZ, E.; *Cation miscibility in CeO_2-ZrO_2 oxides with fluorite structure. Combined TEM, SAED and XRD Rietveld analysis.* Journal of Materials Chemestry, 16(43), 2006

[18] NAKAHIRA, A.; MURAKAMI, T.; KUDOU, T.; MATSUSHITA, T.; HONMA, T. *Fabrication and evaluation of High Performance 12Ce-ZrO_2/3Y-ZrO_2 composites for an Implant.* Journal of the Ceramic Society of Japan, 114, 2006; pp 1076-1080.

[19] JANSEN, S.; WINNUBST, A.; HE, Y.; VERWEIJ, H.; VAN DER VAST, P.; DE WITH, G. *Effects of Grain Size and Ceria Addition on Agening Behaviour and Tribological Properties of Y-TZP Ceramics.* Journal of European Ceramic Society, 18, 1998; pp 557-563.

[20] KRUTH, J.; LEU, M.C.; NAKAGAWA, T. *Progress in Additive Manufacturing and Rapid Prototyping*. CIRP Annals- Manufacturing Technology, vol. 47, 1998; pp 525-540.

[21] KERNS, J. *3D Pringint Tips and Tech*. Machine Design, 10, 2015; pp 53-57.

[22] CRESPO, F; *Effect of porosity on the mechanical properties of zirconia based ceramics obtained via 3D printing.* Barcelona, ETSEIB – TFG, 2016.

[23] http://www.themethodcase.com/fabclay-by-sasha-jokic/ Visited 14th of May of 2016.

[24] UTELA, B.; STORRI, D.; ANDERSON, R.; GANTER, M. *A review of process development steps for new material systems in three dimensional printing (3DP).* Journal of manufacturing processes, 10, 2008; pp 96-104.

[25] ELBERT, J.; ÖZKOL, E.; ZEICHNER, A.; UIBEL, K.; WEISS, Ö.; KOOPS, U.; TELLE, R.; FISCHER, H. *Direct Inkject Printing of Dental Prostheses Made of Zirconia.* Journal of Dental Research, 88, 2009; pp 673-676.

[26] BAUER, J.; HENGSBACH, S.; TESARI, I.; SCHWAIGER, R.; KRAFT, O. *High-strength cellular ceramic composites with 3D microarchitecture.* Insitute for Applied Materials and Karlsruhe Nano Micro Facility, Karlsruhe Institute of Technology. Germany, Vol. 111 (7), 2014; pp 2453-2458.

[27] ESCOBAR, E.; JEONG, C.; KAY, L.; KISAILUS, D.; ZAVATIERI, P. *Analysis of the mechanical response of biomimetic materials with highly oriented microstructures through 3D Printing, mechanical testing and modeling.* Journal of mechanical behavior of Biomedical Materials, 48, 2015; pp 70-85.

[28] FAES, M.; VALKENAERS, H.; VOGELER, F; VLEUGELS, J.; FERRARIS, E. *Extrusion-based 3D Printing of ceramic components.* 3rd CIRP Global Web Conference, vol. 28, 2015, pp 76-81.

[29] MUÑOZ TABARES, J.A. *Cambios microestructurales en 3Y-TZP desbastada y su influencia en la degradación hidrotérmica,* Barcelona: ETSEIB – TD, 2010.

[30] VIVANCOS CALVET, J.; BUJ CORRAL, I.; COSTA HERRERO, Ll. *Sistemas de Fabricación*. Barcelona: 2010.

[31] http://kepcoinc.com/downloads/Electro_Polishing/LC_surface-roughness-measurements.pdf Visited 25th of May of 2016.

[32] Aerospace engineering guide, Edition April 2008. TRELLEBORG Sealing Solutions.

[33] CAMPINS FALCÓ, P.; QUEROL PIÑÓN, FM. *Applications in forensic chemestry of diffuse reflectance spectroscopy techniques for the characterization of authenticity of Spanish stamps.* Gaceta internacional de ciencias forenses. Valencia, Vol. 5, 2012; pp 48-75.

[34] http://www.shimadzu.com/an/molecular_spectro/uv/accessory/solidsample/solid.html Visited 5th of June of 2016.

[35] http://www.mikeblaber.org/oldwine/BCH4053l/Lecture02/Lecture02.htm Visited 5th of June of 2016.

[36] ALFARO MOCTEZUMA, P. E.; ÁNGELES MEDINA, F.; OSORNO ESCAREÑO, M.C.; NÚÑEZ MARTÍNEZ, J.M. ; ROMERO ESQUILIANO, G. *Fuerza de mordida: su importancia en la masticación, su medición y sus condicionantes clínicos. Parte I.* ADM Magazine, Mexico, vol. 69, 2011; p 53-57.

[37] ROA, J.J.; TURON-VIÑAS, M.; ANGLADA, M. *Surface grain size and texture after annealing groun zirconia.* Journal of the European Ceramic Society, vol. 36, 2016; pp 1519-1525.

APPENDIX

A1 Optical properties

Table A1.a – *Reflectance, transmittance and absorbance for 3Y-TZP95%-5%CeO_2*

95_1450				95_1740			
Wavelength (nm)	**R (%)**	**T (%)**	**A (%)**	**Wavelength (nm)**	**R (%)**	**T (%)**	**A (%)**
250	10.72	0.02	89.28	250	10.74	0.02	89.26
350	10.71	0.01	89.29	350	14.27	0.00	85.73
450	38.34	0.38	61.66	450	37.68	0.01	62.32
550	43.11	1.24	56.89	550	45.33	0.03	54.67
650	44.58	1.55	55.42	650	48.62	0.09	51.38
750	46.98	1.77	53.02	750	50.87	0.19	49.13
850	45.98	1.95	54.02	850	53.00	0.22	47.00
950	46.06	1.58	53.94	950	52.45	0.71	47.55
1050	47.05	2.20	52.95	1050	52.57	0.61	47.43
1150	47.03	1.83	52.97	1150	52.57	0.66	47.43
1250	46.97	2.26	53.03	1250	52.42	0.80	47.58
1350	47.67	2.36	52.33	1350	53.59	0.24	46.41
1450	51.84	2.20	48.16	1450	58.53	0.10	41.47
1550	48.69	2.68	51.31	1550	55.67	0.22	44.33
1650	48.44	1.94	51.56	1650	54.67	-0.55	45.33
1750	48.92	1.23	51.08	1750	56.41	-1.00	43.59
1850	50.75	2.18	49.25	1850	58.55	0.85	41.45
1950	69.65	0.62	30.35	1950	83.42	1.32	16.58
2000	64.82	4.00	35.18	2000	69.07	2.13	30.93

Table A1.b – *Reflectance and absorbance for 3Y-TZP90%-10%CeO_2*

90_1450			90_1740		
Wavelength (nm)	**R (%)**	**A (%)**	**Wavelength (nm)**	**R (%)**	**A (%)**
250	7.66	92.35	250	7.23	92.77
350	10.18	89.82	350	8.15	91.85
450	29.51	70.49	450	31.44	68.56
550	34.75	65.25	550	38.31	61.69
650	39.67	60.33	650	42.22	57.78
750	44.08	55.92	750	45.18	54.82
850	47.47	52.53	850	44.39	55.61
950	50.64	49.36	950	46.24	53.76
1050	51.15	48.86	1050	45.99	54.01
1150	52.69	47.31	1150	46.31	53.69
1250	53.10	46.90	1250	46.19	53.81
1350	54.76	45.24	1350	47.26	52.74
1450	59.72	40.28	1450	51.23	48.77
1550	57.07	42.93	1550	48.44	51.56
1650	54.78	45.22	1650	48.48	51.52
1750	55.91	44.09	1750	48.93	51.07
1850	58.73	41.27	1850	50.09	49.91
1950	78.12	21.88	1950	66.98	33.02
2000	70.40	29.60	2000	62.99	37.01

Table A1.c – *Reflectance and absorbance for 3Y-TZP80%-20%CeO_2*

80_1450			80_1740		
Wavelength (nm)	**R (%)**	**A (%)**	**Wavelength (nm)**	**R (%)**	**A (%)**
250	7.06	92.94	250	7.78	92.22
350	8.90	91.10	350	9.26	90.74
450	25.05	74.95	450	36.31	63.69
550	29.98	70.02	550	42.69	57.31
650	32.83	67.17	650	46.31	53.69
750	35.24	64.76	750	49.80	50.20
850	35.63	64.37	850	51.57	48.43
950	35.96	64.04	950	51.46	48.54
1050	35.89	64.11	1050	50.96	49.04
1150	36.01	63.99	1150	51.58	48.42
1250	36.00	64.00	1250	51.91	48.09
1350	36.64	63.36	1350	53.37	46.63
1450	39.84	60.16	1450	57.66	42.34
1550	37.38	62.62	1550	54.60	45.40
1650	38.18	61.82	1650	54.06	45.94
1750	38.44	61.56	1750	55.17	44.83
1850	38.94	61.06	1850	55.97	44.03
1950	52,90	47.10	1950	69.50	30.50
2000	46.40	53.60	2000	75.07	24.93

Table A1.d – *Reflectance and absorbance for 50_1740 sample*

50_1740		
Wavelength (nm)	**R (%)**	**A (%)**
250	6.33	93.67
350	8.99	91.01
450	22.98	77.02
550	26.81	73.19
650	29.56	70.44
750	32.59	67.41
850	33.44	66.56
950	32.28	67.72
1050	33.21	66.79
1150	32.91	67.09
1250	33.13	66.87
1350	33.68	66.32
1450	36.20	63.80
1550	34.94	65.06
1650	33.72	66.28
1750	32.72	67.28
1850	35.54	64.46
1950	46.20	53.80
2000	42.85	57.15

B1 Vickers hardness

Table B1 – *Vickers hardness values.*

	Indentation 1		Indentation 2		Indentation 3		Indentation 4		FINAL
	d (µm)	HV	d (µm)	HV	d (µm)	HV	d (µm)	HV	HV
95_1450	40.8	1114.4	44.0	952.8	43.1	997.9	45.5	897.1	990.5
95_1740	46.5	857.0	52.9	658.3	49.3	762.8	59.8	518.3	699.1
90_1450	50.0	741.7	46.0	873.4	55.3	605.3	53.5	648.6	717.3
90_1740	40.6	1126.8	44.9	913.7	44.5	938.2	44.7	928.9	976.9
80_1450	63.5	459.4	44.5	933.7	47.8	812.7	48.3	796.5	750.5
80_1740	46.3	866.2	45.7	885.0	45.7	889.3	44.8	923.9	891.1
50_1740	90.9	224.3	88.9	233.5	87.4	243.0	88.7	235.8	234.1